U.S. DEPARTMENT OF ENERGY

PNNL-22813

Prepared for the U.S. Department of Energy
under Contract DE-AC05-76RL01830

Modeling and Simulation Capabilities for the Evaluation of Microgrids

KP Schneider
TL Williams
FK Tuffner
Y Zhang
MJ Rice
BB Van Kirk

September 2013

Pacific Northwest
NATIONAL LABORATORY

DISCLAIMER

PACIFIC NORTHWEST NATIONAL LABORATORY

operated by

BATTELLE

for the

UNITED STATES DEPARTMENT OF ENERGY

under Contract DE-AC05-76RL01830

Printed in the United States of America

Available to DOE and DOE contractors from the Office of Scientific and Technical Information,

P.O. Box 62, Oak Ridge, TN 37831-0062; ph: (865) 576-8401 fax: (865) 576-5728 email: reports@adonis.osti.gov

Available to the public from the National Technical Information Service,

U.S. Department of Commerce, 5285 Port Royal Rd., Springfield, VA 22161

ph: (800) 553-6847 fax: (703) 605-6900

email: orders@ntis.fedworld.gov online ordering: http://www.ntis.gov/ordering.htm

 This document was printed on recycled paper.

(9/2013)

PNNL-22813

Modeling and Simulation Capabilities for the Evaluation of Microgrids

KP Schneider TL Williams
FK Tuffner Y Zhang
MJ Rice BB Van Kirk

September 2013

Prepared for
the U.S. Department of Energy
under Contract DE-AC05-76RL01830

Pacific Northwest National Laboratory
Richland, Washington 99352

Table of Contents

Table of Figures

Table of Tables

1 Introduction

Microgrids have been deployed around the world because of their ability to provide electricity in urban and remote locations with exceptionally high levels of reliability. One potential source of increased reliability is that the generation sources are located near the end-use loads and they are not reliant on a large interconnected transmission system. While this limits the generation resources to a particular load, it removes the larger, interconnection network that could experience issues. The generation sources in microgrids can be traditional units or a combination of traditional units and renewables units [1]. In the United States, microgrids are primarily deployed to increase the reliability of high value critical end-use loads; the average residential customer is not supplied by a microgrid [1]. This is due to the high cost of designing and operating microgrids, which is partially due to the lack of effective simulation and analysis tools.

As part of the United States Department of Energy, Office of Electricity Delivery and Energy Reliability (DOE/OE) agenda, there are program level goals for both smart grid and microgrids; both have target dates of 2020. The microgrid analysis efforts of DOE/OE are a subset of the smart grid program. Table 1.1 and Table 1.2 show the smart grid and microgrid program goals for DOE/OE [1].

Table 1.1: DOE/OE smart grid goals for 2020

Smart Grid (2020)	
Goal 1	20% reduction in SAIDI
Goal 2	20% reduction in load factor
Goal 3	>98% reduction in outages

Table 1.2: DOE/OE microgrid goals for 2020

Microgrid (2020)	
Goal 1	Cost parity with DGs and UPSs
Goal 2	20% improvement in efficiency
Goal 3	>98% reduction in outages
Goal 4	>20% reduction of emissions

To support the goals of the DOE/OE microgrid program, and parent smart grid program, the Pacific Northwest National Laboratory (PNNL) developed four simulation and analysis capabilities in the open-source simulation environment GridLAB-D. The first capability focuses on increasing the utility of microgrids by using them as a resource for restoration and recovery. This first capability is a joint effort between PNNL and Washington State University (WSU). The second capability is a modeling framework that enables a user to improve generic device models based on hardware measurements. This framework is intended to reduce the cost of design and deployment of microgrids by allowing more detailed simulations and design evaluations before actual hardware is purchased or deployed. The second capability is a joint effort between PNNL and Oak Ridge National Laboratory (ORNL). The third capability is an

integration of GridLAB-D capabilities with Sandia National Laboratories' (SNL) Technical Management Optimization (TMO) tool. By building an interface between GridLAB-D and TMO it is possible to perform the high-level optimization function in TMO while enforcing feasibility constraints via GridLAB-D. This capability is designed to provide an integrated tool set that reduces design costs for microgrids. The fourth capability is an Automatic Meter Infrastructure (AMI) diagnostic system. This capability is designed to improve the reliability of microgrids, and distribution systems in general, by performing diagnostic analysis on data that is already being collected by utilities.

All of the collaborations mentioned were parallel efforts to meet the DOE/OE goals. WSU generated the reconfiguration algorithm and implemented it separately. ORNL tested the inverter hardware and provided PNNL with measurement values. SNL is performing the integration with the TMO tool, with PNNL just providing overall support. While related, no direct collaborative work was performed on any of the sections within this report. This report contains only the PNNL-performed work. Parallel reports are expected to be published independently from the collaborating entities on their work towards the overall DOE/OE goals.

This document is organized as follows. Section 2 examines the potential to use microgrids as a resiliency resource. Section 3 discusses the modeling framework developed in cooperation with ORNL and Section 4 discusses the GridLAB-D TMO interface developed in cooperation with SNL. Section 5 details the AMI base diagnostic system and Section 6 contains the concluding comments.

2 WSU Microgrid

Recent natural disasters and extreme weather conditions in the United States have prompted investigations into how to make the power grid more resilient to such events. One method for improving the resiliency of the power grid is with the use of microgrids. When a natural disaster or event removes the main transmission power supply to a grid, local resources can be used to power critical loads until service is restored.

To investigate the benefits of microgrid operation on improved power system resilience, PNNL partnered with the Washington State University (WSU) in Pullman, Washington to investigate transient considerations (behaviors that change on the order of milliseconds) on the reconfiguration operations associated with such microgrid operations. During an emergency, the grid could be reconfigured to connect the generation resources with the desired loads. Since microgrid generation is much smaller than the larger grid resources, improper rerouting of power can overload equipment or trigger protective mechanisms. This can prevent power from getting to the desired locations, as well as exacerbate any problems already present in the system as a result of the emergency.

2.1 Approach

To facilitate exploring the reconfiguration impacts on a microgrid and how affects overall resiliency, portions of the task were divided between PNNL and WSU. PNNL would create a model of the microgrid system (the city of Pullman, Washington) and develop the capabilities necessary to simulate the microgrid on a millisecond timescale. WSU would create the reconfiguration algorithm, which considers the electrical constraints, topological constraints, and any dynamic constraints on the system. The two portions of the project are combined inside the GridLAB-D simulation environment and different scenarios examined.

2.1.1 Transient Impacts

One of the primary areas of concern with microgrid operations is the transient behavior of various operations. Closing a sectionalizing switch and enabling a significant portion of the system could result in a frequency drop (associated with the generators trying to “catch up” or being overloaded), which may lead to generators and other loads tripping offline. Behaviors, such as this frequency drop, need to be examined and incorporated into any reconfiguration schemes to ensure that the microgrid operation is improving resiliency, not degrading it.

Under the current fiscal year work, two primary categories of transient behavior were of interest. The first is the transient behavior of the backup generation sources on the system. During the microgrid operations and reconfiguration actions, the backup generators will need to respond to changes in the system and maintain power production. Insights into how these generators respond to various actions on the system can help influence operations and ensure no damage to any equipment occurs.

The second transient behavior of interest is the voltage and current flow into distribution lines and transformers as they are switched back into service and energized. The initial inrush current into a line or transformer could overwhelm the backup generation or interfere with their control systems. With this behavior modeled, the impacts on the generation, as well as how it impacts the microgrid stability during reconfiguration, can be examined.

2.1.1.1 Transient model of generators

Transient modeling capabilities for the generators required augmenting existing generator capabilities within GridLAB-D. As part of the work in FY13, unbalanced electromechanical transient models for diesel distributed generators were implemented within GridLAB-D. These models capture millisecond-level interactions of the diesel generators with the power system. The WSU campus microgrid deploys one diesel generator and two natural gas generators, all of which could be represented by the existing model.

Of greater importance for the modeling task is obtaining accurate parameters for the generation resources on the WSU campus. Utilizing data sheets and input from the original vendor, a rough set of parameters were obtained for the models. To improve the accuracy of these parameters, several tests will be performed on the WSU generators. While non-invasive in nature (only measurements during normal operation are used), these tests will refine the datasheet parameters to more accurately represent how the system would behave during microgrid operations. These tests are expected to complete during the next fiscal year (FY14).

2.1.1.2 Transient model of connecting devices

One of the greatest concerns for microgrid operation of the Pullman system is how energizing larger sections of distribution lines, transformers, and general cold-load-pickup procedures will affect the system. In particular, a very large unknown exists with longer sections of line and de-energized transformers. When reactivated, the inrush current associated with reactivating these devices may overwhelm the limited generation resources.

Traditional modeling of inrush current is accomplished using electromagnetic-level simulations. However, GridLAB-D operates in a phasor-equivalent representation, which does not lend itself well to electromagnetic simulation. To capture these effects in a manner compatible with GridLAB-D, a method for capturing dynamic effects in a phasor format was needed.

Research conducted in [2] details such an approach. Using a concept known as dynamic phasors, transient behavior of power systems can be modeled without requiring microsecond-level simulations of electromagnetic effects. Dynamic phasors are built off the fundamental assumption of (2.1):

$$\left\langle \frac{dx}{dt} \right\rangle_k = \frac{dX_k}{dt} + j\omega_s X_k, \tag{2.1}$$

where X_k represents the frequency domain representation of a time-domain response, ω_s represents the sampling frequency (or base sampling time), t is time, and k represents a multiple of the sampling frequency. As a simple comparison to existing phasor methods, the dynamic phasor extends them beyond the 60 Hz assumption to many different frequencies. By effectively creating a phasor for each fundamental component of the signal (similar to a Fourier series), the transient impacts can still be represented in phasor notation, just in more terms than the conventional 60 Hz-based phasor notation.

Two basic models needed to be implemented to capture microgrid reconfiguration impacts: transformer magnetizing currents and distribution line-charging currents. Both can be lumped under generic “inrush” current models, but have two fundamental equation sets. Traditional electromagnetic equations were converted into dynamic phasor notation for implementation into GridLAB-D. The details of the equations can be found at [3]. Simulation results for the implementation are found later in this section of the report.

2.1.2 Modeled System

To provide a realistic and compelling example of using a microgrid as a means to improve grid reliability and resiliency, the grid for a portion of the city of Pullman, Washington was selected. Figure 2.1 shows a rough topology of the portion of the city modeled. During a long-term disaster, it may be possible to use the generation resources located on the WSU campus to power critical loads at the hospital and city hall (the city’s disaster relief command center). However, the system is not normally operated in this manner, so reconfiguration steps and additional impacts on the system need to be examined. By using a realistic system model, the PNNL and WSU analysis will consider realistic impacts for operating an existing grid in a microgrid manner.

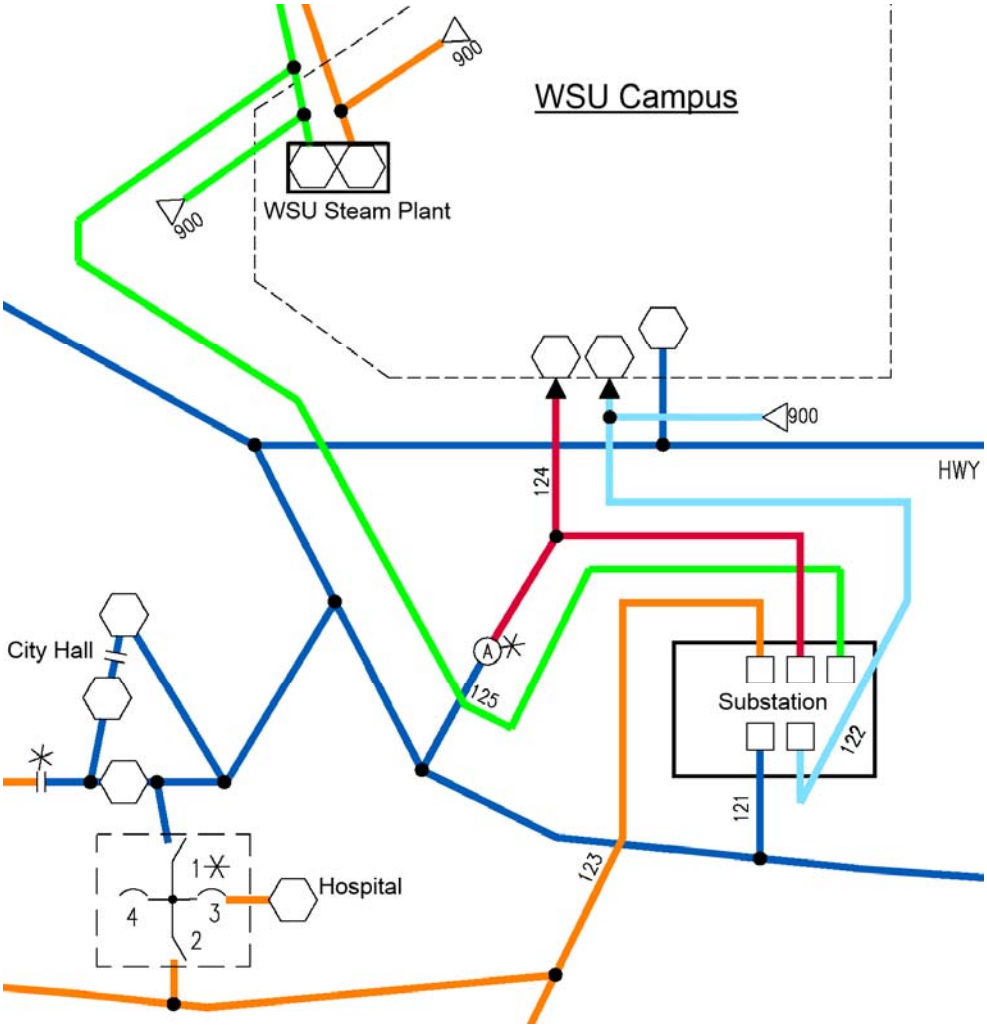

Figure 2.1: Pullman, Washington System Modeled

2.1.2.1 Topology

The portion of the Pullman system proposed for microgrid operation is spread across at least three feeders, with two more providing connections that may be useful for alternative paths between resources. All of the relevant feeders are fed through a common substation, with appropriate switchgear inside to provide connections. Not shown in Figure 2.1 are additional paths and switchgear within the WSU campus, which could allow the 125 feeder to be connected to the 121, 122, and 124 feeders through the campus network.

Generation resources considered are all on the WSU campus and located at the WSU Steam Plant. Two natural gas generators and one diesel generator provide backup power to the campus, but will be utilized in this study to supply energy to the hospital and city hall. The diesel generator is connected more for internal campus power and critical resources, but can be connected to the other generators through existing switchgear.

The first desired load on the system is the Pullman hospital. While the hospital does have its own on-site backup generation, there are a few scenarios that could warrant connection with the WSU generation resources. The most dire of these are if the on-site generation is unavailable or their on-site fuel supply has been exhausted. However, another potential benefit is sharing overall generation resources for greater efficiency. Rather than loading several generators at half-power, greater efficiency may be possible by loading specific generators higher and shutting others down. Such concepts are being explored in other Department of Energy projects and may influence the reconfiguration options explored in the WSU grid.

Regardless of the circumstances for the reconfiguration, the scenario proposed assumes that either this generator is unavailable, or the emergency condition has exceeded their on-site fuel supply. The hospital connects to the grid via feeder 123. However, there are connections to feeder 121, which allow the hospital to continue to receive power if something occurs on feeder 123.

The second desired load, city hall, is tied exclusively to feeder 121. Along with the city hall, many other large loads are fed by feeder 121, so their impacts on the system must be considered as well. Switchgear and “manual” techniques (disconnecting loads via meter removal or line disconnects) may be needed to ensure only critical loads are served by the microgrid resources.

2.1.2.2 Generators

For the microgrid scenario proposed, the WSU campus has three generators that will be considered. The first of these is a backup diesel generator that serves the “life critical” loads within the WSU campus. This generator is rated at 2.1 MVA peak capacity, with 1.75 MW available for active power generation normally. The diesel generator operates as an isochronous generator, but maintains the “last interconnect” frequency, rather than a 60 Hz nominal.

The two remaining generators are natural-gas burning generators typically used as backup power for the steam facilities within WSU. These two generators are both rated at 1.563 MVA, with 1.1 MW rated real power output. As with the diesel generator, these operate with an isochronous governor, maintaining the last interconnect frequency seen.

Under standard operating conditions, only generators 2 and 3 (one natural gas and the diesel generator) are operated in parallel. For the microgrid scenario, all three generators may be operating in parallel at the same instance in time. As such, special considerations will need to be given to ensure that paralleling all three generators is still within the feasibility constraints of the microgrid operations.

2.1.3 Modeled System

As part of the joint nature of the collaboration, students and professors at WSU investigated reconfiguration algorithms for the Pullman microgrid. Dynamic simulations of the WSU microgrid with Pullman distribution feeders were performed in MATLAB/Simulink to illustrate the feasibility of using microgrids to enhance reliability of a distribution system. A restoration algorithm based on graph theory for distribution systems with microgrids has been developed. A restoration software module has been developed using MATLAB and GridLAB-D. In addition, a reliability analysis for a simplified Pullman-WSU system has been completed.

2.2 Simulations

The WSU-developed reconfiguration algorithm continues to be refined. Next steps include the inclusion of dynamic impacts of the line and transformer impacts mentioned earlier in this section. While the reconfiguration algorithm is not fully completed, initial simulations showing the dynamic phasor implementation within GridLAB-D were conducted.

Figure 2.2 shows the phasor representation of the current during the closing of a sectionalizing switch on part of the Pullman, Washington model. This section of line was previously de-energized, representing a complete loss of generation. After reconfiguring the grid to utilize the WSU generation resources, the restoration process begins by slowly switching in other sections of the distribution system. Notice the inrush current at 90 amps, despite the fact that this line is completely unloaded. This particular line is rated at roughly 6 kV, which represents an inrush peak power of over 500 kVA. With a longer section of line, this impact could be even more significant, resulting in a far greater transient load on the generators and system equipment.

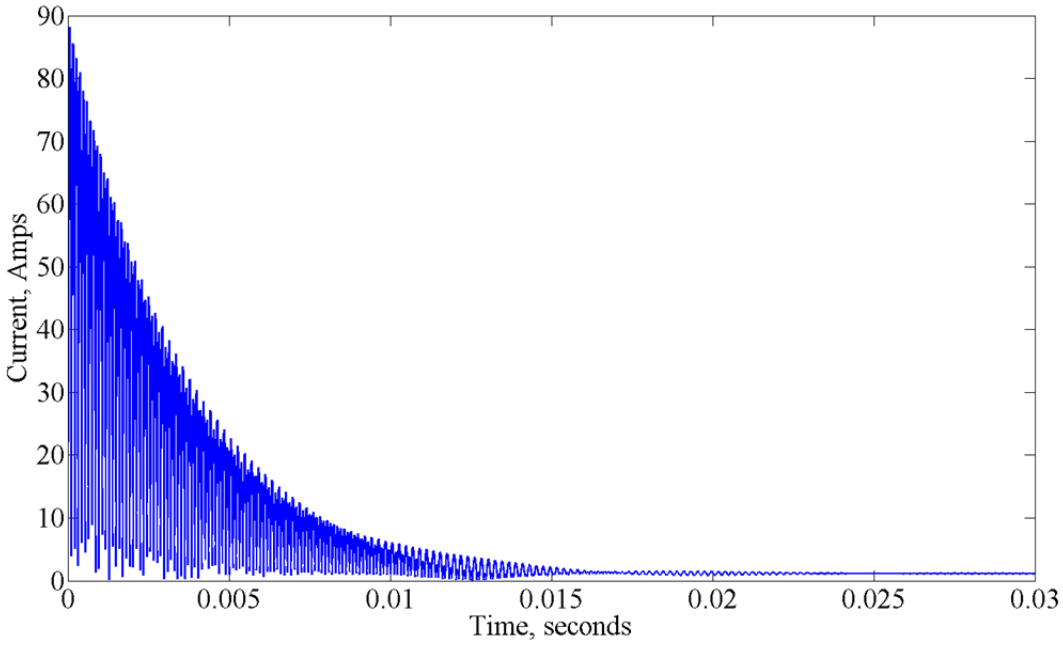

Figure 2.2: GridLAB-D simulation results of overhead line current during closing of nearby sectionalizer

Figure 2.3 shows the current for one phase of an unloaded distribution transformer being switched into service during a restoration operation. Much like the line example before, this transformer was de-energized while the microgrid was reconfigured. Once a nearby sectionalizer is closed, the magnetic field within the transformer must be restored, resulting in the current shown in Figure 2.3. This particular example is not as dire as the overhead line, but mainly due to the unloaded nature of the transformer. With a connected load, the inrush could be significantly higher and have a significant impact on the limited generation resources.

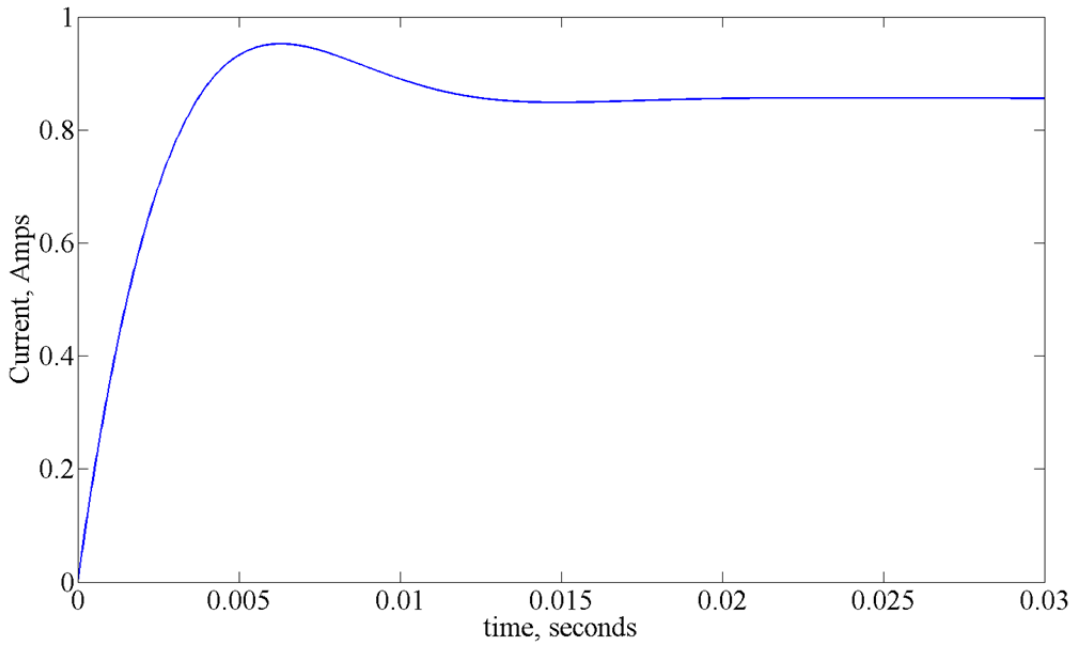

Figure 2.3: GridLAB-D simulation results of transformer current during closing of nearby sectionalizer

The results shown in Figure 2.2 and Figure 2.3 show the result of closing two sectionalizer switches within the system. The full reconfiguration of the system to deliver power from the WSU generation resources to the Pullman hospital and city hall will require several such events. Utilizing the reconfiguration algorithm in development by WSU, the system will be able to sequence the reconfiguration factoring in the transient impacts associated with energizing the out of service devices. Factoring in these transients and successfully reconfiguring the existing distribution resources to serve the critical public services will demonstrate the increased resiliency such a microgrid can offer.

2.3 Continued Research

The work accomplished for FY13 provides a lot of the basic capabilities needed to explore further microgrid and resiliency concepts. Further research in the area will examine specifics of the reconfiguration algorithms, including how to factor in the inrush currents and other dynamic considerations. Overall voltage stability, generation mix changes, and overall topology will be considered and optimized towards serving critical loads on the system.

Another related research topic involves investigating and including direct impacts on protective devices within the microgrid. Once disconnected from a larger bulk power system, existing flow directions and protection settings may no longer be valid, and may actually decrease overall reliability and resilience. Incorporating ground and neutral flows explicitly, along with more explicit models of protective devices, will allow these influences to be explored. The impacts and lessons can integrate with the reconfiguration work to help ensure the new topologies increase the overall resilience of the microgrid system.

3 ORNL Modeling Framework

Examining and understanding the impacts of various microgrid technologies is essential to fully quantifying the benefits and ensuring deployments will move towards the overall DOE microgrid goals. While a direct field demonstration is one approach, it is not always cost effective or feasible for every scenario. Software simulations can provide insight into how the components will interact with each other and the larger system, as well as help quantify the benefits of an installation. However, the estimates and information from simulation are only as good as the underlying models and assumptions.

As part of the FY13 DOE/OE program, PNNL developed a modeling framework, or guided process, to help model hardware devices in sufficient detail for such studies. In collaboration with Oak Ridge National Laboratory (ORNL), PNNL modeled an ORNL hardware inverter inside the GridLAB-D software environment using the designed framework. The created framework and this specific implementation example provide guidelines for future model development and the evaluation of microgrid technologies before their deployment.

3.1 Framework

Creating a software model of a physical device is a common approach to examining larger deployments of equipment, or examining impacts under conditions that the actual system cannot normally operate. However, the process of capturing all the relevant information from the hardware testing has many difficulties. This includes ensuring that all information is collected and sufficient levels of detail have been considered. The modeling framework developed helps frame many of these questions, and suggests an order of progression in creating the software model.

The framework itself is presented in a web-based format and can be viewed at [4]. Figure 3.1 shows the flowchart representation of the modeling framework. Each block contains a summary of the step in the framework, as well as potential questions that should be answered before moving forward in the modeling process. Blocks are also color-coded for different facets of the modeling process, whether it is the model itself, the hardware validation, or even the overall scoping of what the model hopes to represent. This provides a decision-point-based process that helps ensure relevant questions and considerations are answered at the proper point in the modeling process. The website includes two additional examples: a simple AC-to-DC rectification circuit, and the more detailed inverter model described briefly in the next section.

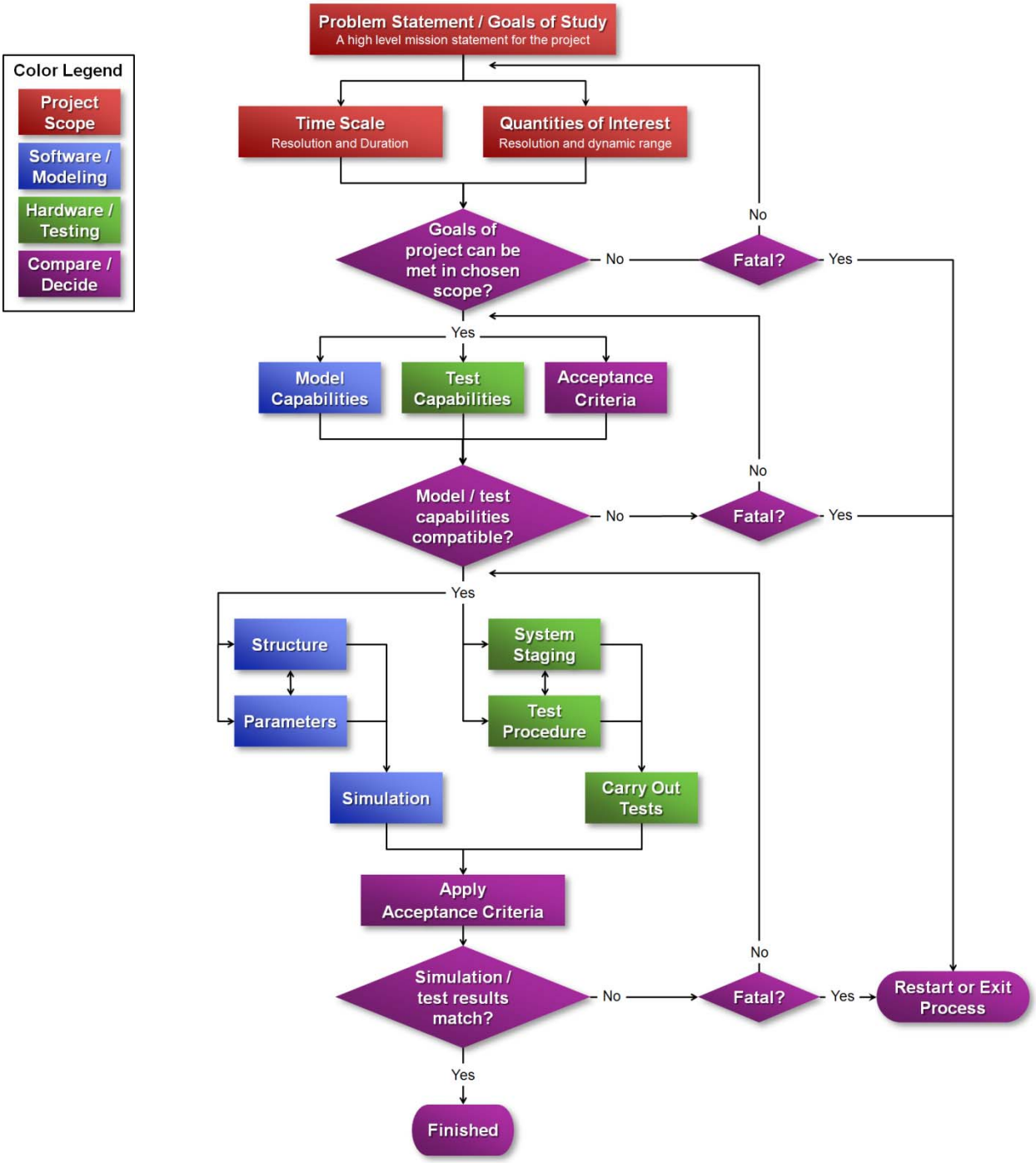

Figure 3.1: Modeling Framework flowchart

3.2 Inverter Modeling

To demonstrate the framework process, and to expand the underlying capabilities of the GridLAB-D software, PNNL and ORNL collaborated to produce a model of an advanced four-quadrant inverter. The modeling framework guided the process of taking the physical hardware device and creating a GridLAB-D software model for further simulation. Validation portions of

the framework were conducted using hardware testing data provided by ORNL from testing within their Distributed Energy Communications and Controls (DECC) Laboratory.

3.2.1 Modeling Approach

The first two steps of the framework required scoping out the overall capabilities of the model, including considerations about the testing capability of the DECC facility. Sample rates are sufficiently high and testing capabilities were conducive to modeling the transition of the inverter from grid-tied operation to islanded operation down to millisecond timescales. This model will be useful in examining the impacts of overall microgrid stability when the system transitions to stand-alone operation.

Continuing with the framework structure, the modeling process and hardware testing process were outlined. As indicated earlier, hardware testing was conducted by ORNL staff within the DECC facility. The ORNL staff outlined all equipment staging and test procedures and performed the data acquisition for the different test scenarios. Final data was provided to PNNL for both initial parameter estimates and validation of the software model.

With the details of the implementation and limitations of the ORNL hardware tests known, the GridLAB-D software model began to take shape concurrent with the hardware tests. Due to the timescales within GridLAB-D and the desired test scenarios, more complicated electromagnetic transient models of the inverter were quickly abandoned. The final implementation was based upon models derived and described in [5]. This implementation focuses on the millisecond-level transients of the inverter operating in microgrid configurations. Details of the final implementation are available on the model webpage [5].

The final aspect of the modeling framework involved comparing the software model with the actual hardware tests. The results of this comparison are shown in the next subsection. Per the original scoping requirements, amplitudes of voltage, current, and power waveforms were required to be within 1% of the hardware measurements. These acceptance criteria are compared at each timestep, ensuring the underlying behavior is occurring with a temporal component in line with the actual hardware.

3.2.2 Simulation

As part of the modeling framework, the results of the software model are compared against the measured hardware results. Figure 3.2 shows an overlay of the real power output of the ORNL inverter and the GridLAB-D model for a grid-separation event. As the figure shows, there are some significant discrepancies. The steady-state values align (before and further after the event at 0.25 seconds), but the actual transient period is very different. Internal parameters that were initially thought to be known are different in the two models. While the steady-state results are a good representation for large-time studies, any usage of the sub-second behavior would require further refinement of those constants.

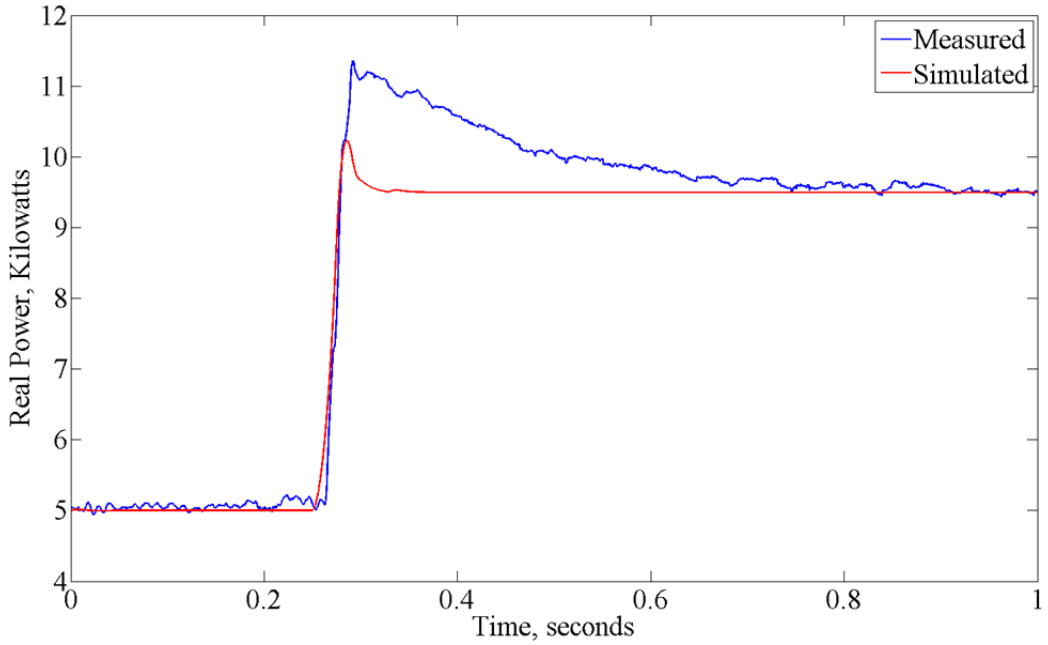

Figure 3.2: Simulation and hardware test results of output power of inverter during islanding event

Further validation occurred against the terminal voltages for the same event. Figure 3.3 shows the overlay of the hardware tests and simulation results for the output voltages. Once again, the steady-state values are nearly identical, but the transient portions show significant differences. For millisecond-level studies, further testing and refinement of internal characteristics are necessary before the model is valid.

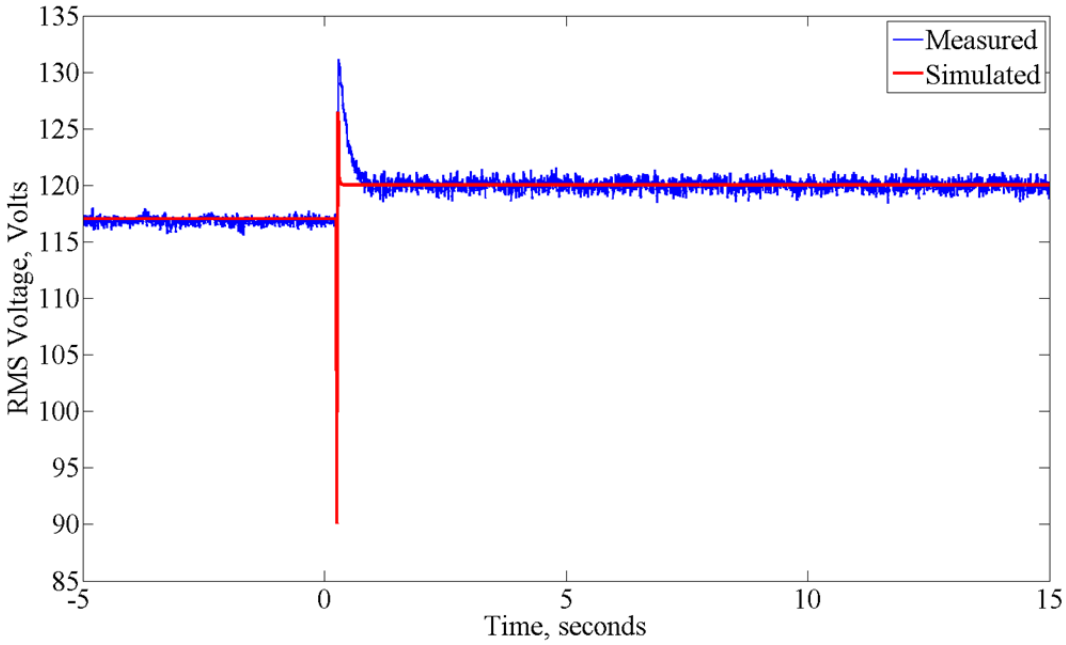

Figure 3.3: Simulation and hardware test results of system voltage of inverter during islanding event

With the results highlighted in Figure 3.2 and Figure 3.3, questions are raised about the validity of the model. This model clearly does not meet the acceptance criteria put forth, and requires further iterations. Details on the equations and further results are available at [5]. In this case, it is the inclusion of suspect information that requires further study. The framework process is still valid, and indicates acceptance is not met and further study is required.

3.3 Further Research

While the main goal of the framework design was to help model the ORNL-tested inverter, the framework is useful for many other models. Through further applications, suggestions and refinements will be incorporated into the framework to provide further guidance for future modeling work. To help aid this refinement, Seattle University will utilize the framework for their senior-level capstone engineering course. With a broader audience utilizing the framework, it is expected the feedback will help improve the question set and overall framework usefulness.

4 TMO Integration

With the increased resiliency microgrids can offer distribution resources, interest in deploying such capabilities is also increasing. However, many considerations must go into deploying such a microgrid, both electrical and economic. Sandia National Laboratories are utilizing their Technology Management Optimization software to help answer such questions. Incorporating a variety of constraints, the TMO software helps examine operation characteristics of prospective microgrids.

Existing TMO studies utilize only a basic energy balance. As long as generator output was the same as desired load, the system was considered a valid electrical solution. Impacts of the specific topology and how certain outages may influence the results have not been directly examined. To incorporate this constraint, the TMO needs to perform a powerflow solution and check the viability of each scenario. Rather than duplicate existing tools, SNL chose to integrate the existing capabilities of GridLAB-D to meet this constraint. With the two software tools successfully communicating, the results obtained from TMO analyses will more accurately explore the feasibility of different microgrid scenarios.

4.1 Integration

Initial integration will occur using a socket-based interface for exchanging information between GridLAB-D and the TMO software. Status of various elements, load levels, and generator outputs will be passed to GridLAB-D in a predetermined sequence of messages. GridLAB-D will execute a load flow and report any electrical violations (equipment overloads, lack of voltage support, or outright infeasibility) back to the TMO for consideration in its optimization process. Such an interaction will occur for thousands of different topological and equipment considerations as the TMO explores the parameter space.

4.2 Expected Simulation Results

GridLAB-D and TMO integration results are not immediately available for this report. Successful integration will be demonstrated during a November 2013 demonstration of the integrated TMO tool suite. The integration of GridLAB-D and other tools will be part of this demonstration. Intermediate simulation results are simple powerflow outputs, which do not represent any significantly novel results. However, their integration into TMO will result in a better-constrained, more realistic representation of the feasibility of different microgrid structures.

5 AMI Diagnostics

One of the greatest challenges to operating electric distribution systems is the lack of a direct monitoring capability; this is true of traditional distribution systems and microgrids. When a microgrid is deployed it is likely that equipment will remain in place for decades with no direct monitoring. The result is that the actual condition of the system is not known and may only be discovered during a catastrophic failure while under stress. This type of failure would defeat the purpose of a microgrid. This section will examine a method of using AMI based data to determine the condition of equipment within the microgrid to ensure high reliability operation.

When equipment is deployed, and then left unattended for multiple decades, and operators have no indication of the equipment condition. This is especially true of secondary service transformers and underground cables. After these components are deployed, they are often left in operation until they fail, which results in unplanned outages for end-use customers. Because of the large number of secondary service transformers and underground cables, it is not practical to install monitoring equipment or to perform manual inspections. To address these limitations, utilities often over-build their systems to provide additional safety margins, which result in higher capital construction costs. Even with these increased safety margins it is not uncommon for failures of secondary service transformers and/or underground cables to result in customer outages [6],[7].

While it is not cost effective to install monitoring equipment specifically for the distribution infrastructure, many utilities have deployed Automatic Meter Information (AMI) systems [8]. These systems have been designed to automatically collect billing data and perform remote disconnect functions, but their information has the potential to be used for other applications. One potential application is to determine the current state of distribution system equipment and to track variations in the equipment conditions over time based on AMI data. Specifically, a system can be developed using the AMI data that is routinely reported back to the utility to track the condition of secondary service transformers and underground cables. These tracked equipment parameters can then be integrated into a larger asset management system that will allow utilities to determine when proactive replacement of equipment is warranted. This system will increase the system reliability by reducing unplanned outages, and reduce costs by only replacing equipment when appropriate.

For the complete process, the inputs are the utility-collected AMI data, feeder head power flow, and the most up-to-date planning model, with current operational information such as breaker and switch positions. The output will be a list of secondary transformers and underground cables that are flagged as having abnormal conditions, which warrant potential repair or replacement. To achieve this, the presented methodology is divided into five key steps, each of which is described in the following sections. The five key steps are:

Step 1: Data Collection
Step 2: State Estimation

Step 3: Parameter Error Detection
Step 4: Parameter Estimation and Tracking
Step 5: Cable/Transformer Diagnostic

5.1 Process Description

This section contains a description for each of the five key steps of the proposed methodology.

5.1.1 Step 1: Data Collection Process

There are three classes of input data that must be collected in this step:

1) Distribution feeder planning model: these models are normally maintained by a utility's planning department. They include the topology of the system as well as the type of equipment that is believed to be installed. These models also contain what the electrical parameters of equipment are expected to be, but they do not include information regarding the way parameters change over time.
2) Operational state of distribution feeder: while the planning model contains the equipment that is installed in the system, it is still necessary to know the current operational status of breakers, switches, and jumpers. This information can be obtained from a utility's operations group.
3) Consumption and flow data: necessary data includes AMI data and feeder head power flow. The continual flow of AMI data is normally collected by a utility at 5 to 15 minute intervals. Because the proposed method uses large periods of data, high speed communication is not necessary. 5-minute or 15-minute readings can be collected as infrequently as once a day.

These three classes of input data form the complete input set for the AMI diagnostic system. The first class of data, the planning model, is updated on a semi-annual or annual basis at most. The second and third classes of information are operational values that are continually updated.

5.1.2 Step 2: State Estimation Process

Once the data has been collected, the first step of the analysis is to conduct an unbalanced three-phase state estimation of the system. This is a necessary step because of all of the sources of input data contain sources of error. The state estimation process determines a best fit estimate for the state variables of the system, the magnitude and phase angle of the voltage at each bus. This process uses a standard Weighted Least Squares (WLS) power injection formulation that has been extended to include unbalanced per-phase distribution systems.

The output of this step is a best fit estimate for all of the state variables, and a set of measurement residuals indicating the difference between each measurement and its derived best fit value.

5.1.3 Step 3: Parameter Error Detection Process

Parameter error identification is the process by which the measurement residuals from Step 2 are examined to determine if parameter errors exist. Parameter errors are detected by identifying

multiple residuals with a high sensitivity to a common device parameter, e.g., cable insulation [9].

The output of this step is a list of device parameters that are identified as being outside of the expected values indicated by the planning model. If a parameter is identified, it will be flagged for tracking. It is possible that multiple parameter errors will be identified, in which case multiple parameters will be flagged for tracking. The total number of parameters that can be tracked at a single time will depend on the observability of the system [9].

5.1.4 Step 4: Parameter Estimation and Tracking Process

Once a parameter, or set of parameters, has been flagged as potentially erroneous, an evaluation is performed to determine the best fit value for the parameter. Each time a set of new AMI measurements is collected, the best fit value is recalculated. The string of values is tracked over time to determine if the value is only varying with daily load variations, or if its value is drifting consistently over time. If it is found that the best fit value is constant but different from the modeled value, then this may be an indication of an error in the input data. Specifically, this indicates an incorrect value in the feeder planning model, which is a common occurrence. By updating this value, the input data, i.e., the feeder planning model, will be more accurate in the future. If the value is found to be drifting over time, this may be an indication of a slowly degrading piece of equipment.

The output of this step is an estimate of the drift of the parameter value over time. The next step determines if the drift is acceptable.

5.1.5 Step 5: Cable/Transformer Diagnostic Process

In this section the variation of parameters that are being tracked in Step 4 are compared to known models to determine if their variation is within normal tolerances. If the parameter associated with the physical component is found to be changing in a way that is not consistent with component models or environmental trends, the component will be identified as potentially problematic.

Consider underground cables as an example, which are prone to insulation failures. There are numerous diagnostic methods used to test power cables and transformers in order to ascertain deterioration and/or imminent potential for failure. Most of these tests are designed to be performed offline, which is often not practical or possible. However, the targeted characteristics of some of these tests may also be examined in online tests. For example, one of the more common tests for identifying cable failure is a dissipation factor or $tan\ \delta$ test which estimates the ratio of real to reactive impedance of the cable shunt impedance [10]. While shunt elements are typically modeled in power flow as purely reactive, the model can be expanded to include complex shunt elements. Moreover, a trend in shunt capacitance alone may reproduce a similar trend as that seen in dissipation factor.

5.1.6 Process Flowchart

This section contains the process flowchart for the five key steps of the presented methodology. The specific equations and algorithms used in each block of the chart can be found in Section 5.2.

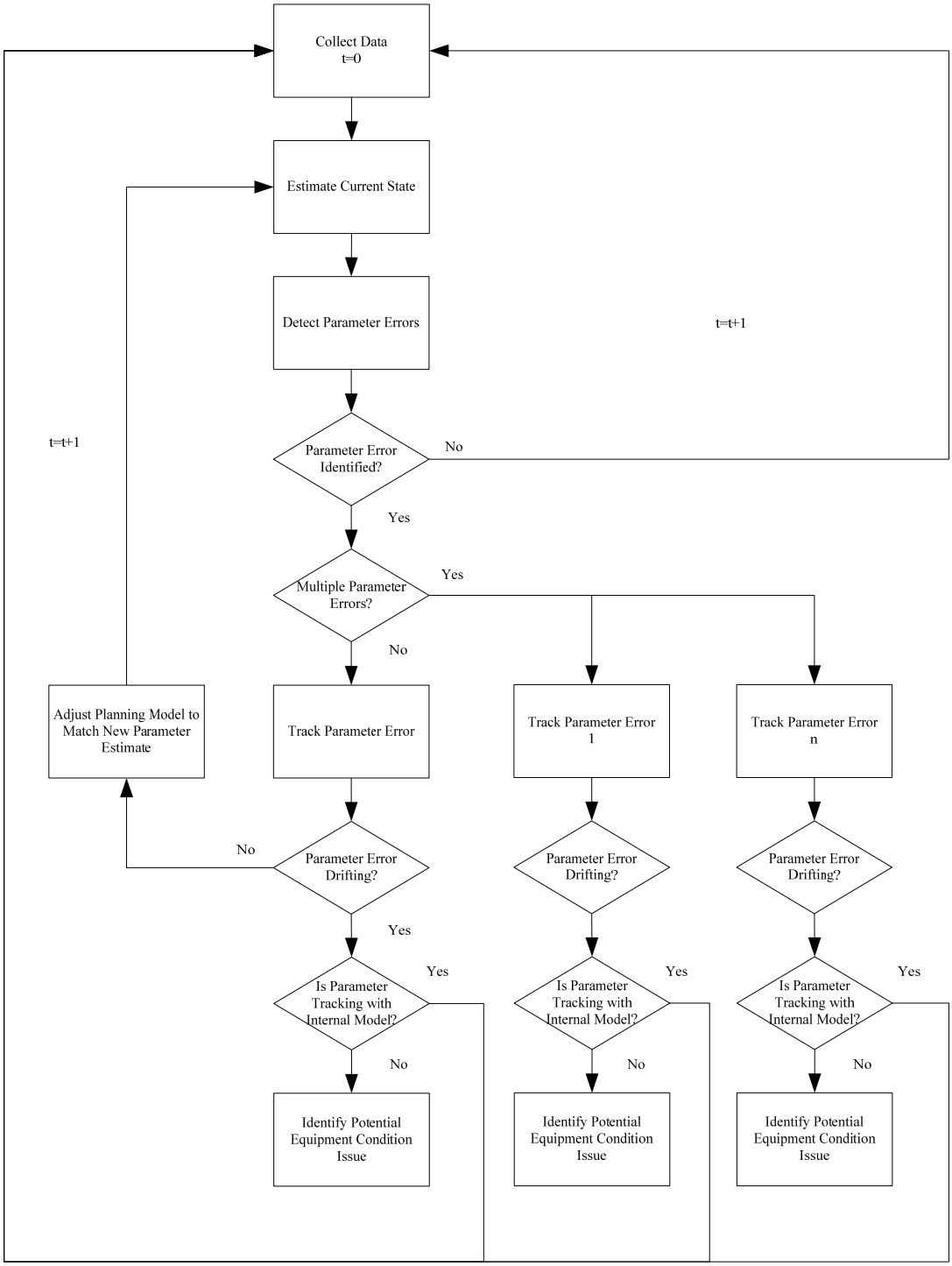

Figure 5.1: Flow chart of evaluation methodology

5.2 Algorithms and Equations

This section contains the algorithms and equations for each of the five key steps of the proposed methodology.

5.2.1 Step 1: Data Collection Algorithms and Equations

For the data collection step there are no specific algorithms developed at this time. A future step will to be the development of a pre-filtering algorithm to sort out "bad" data that may be contained in the AMI data set. This pre-filtering algorithm will be based on existing data analysis techniques.

5.2.2 Step 2: State Estimation Algorithms and Equations

State estimation (SE) for power system has been a well-established process since Fred Schweppe's three-part seminal paper on the topic in 1970 [11], [12], [13]. Equation 3.1 shows the basic formulation for a state estimation solution as presented by Schweppe.

$$x^{k+1} = x^k - [H^T(x^k)R^{-1}H(x^k)]^{-1}\left[H^T(x^k)R^{-1}[z - h(x^k)]\right] \tag{5.1}$$

where:

x^k : The state vector (phase angles and voltage magnitudes)
H^T : Jacobian of measurement equations with respect to state variables
R : Diagonal matrix of weighting values
$h(x^k)$: Vector of measurement equations (functions of measured values)
z : Vector of measurements (line flows and voltage magnitudes)

Equation (5.1) is an iterative solution as is indicated by the superscript indexing of the state vector. The iteration continues until the difference between successive iterations is sufficiently small. This sufficiently small difference is referred to as the convergence criterion. Convergence criteria can vary but generally the quadratic convergence of the WLS method makes it clear when convergence has been achieved.

For the proposed method, the vectors in (5.1) that are of the most interest are z and $h(x^k)$. The z vector is the set of measurements that are the input data to the state estimation problem. In the traditional transmission state estimation, the measurements are one of six types:

1) Real power injections
2) Reactive power injections
3) Real power flows
4) Reactive power flows
5) Voltage magnitudes
6) Current magnitudes

In the balanced transmission application of SE, , it is assumed that the system is balanced and that there is line transposition. Because of this, a single-phase representation can be used to

express each of the measured values as a function of the state variables. For example, the real power injection at bus *i* can be written as a function of the state variables *V* and θ, as shown in (5.2). (5.2) is the element of $h(x^k)$ corresponding to the element of z for the measurement of P_i. Each of the other 5 measurement types can be expressed in similar terms to (5.2).

$$P_i = V_i \sum_{k=1}^{n} V_k [G_{ik} cos\theta_{ik} + B_{ik} sin\theta_{ik}] \tag{5.2}$$

In order to make (5.2) useful for distribution level state estimation, it must be expanded to include each of the individual phases in a distribution system, {a, b, c} [14]. In this representation, the real power injection at bus *i*, for phase *p*, can written as a function of the state variables *V* and θ, as shown in (5.3). Both *p* and *q* represent the phase set {a, b, c}.

$$P_i^p = V_i^p \sum_{k=1}^{n} \sum_{q=1}^{3} V_k^q \left[G_{ik}^{pq} \cos\theta_{ik}^{pq} + B_{ik}^{pq} \sin\theta_{ik}^{pq} \right] \tag{5.3}$$

Equation (5.3) shows the expansion from the traditional single phase, to the more general per-phase formulation, for the power injection at a single phase on a node. This same type of expansion can be made for the other five measurement types, but AMI generally only has the following three measurement types:

1) Real power injections
2) Reactive power injections
3) Voltage magnitudes

By using the same formulation of (5.1), but with the individual elements properly indexed across each of the three phases as shown in (5.3), it is possible to perform an expanded three-phase distribution state estimation. This state estimation then gives the best fit estimate for the angle and voltage magnitude for each of the three phasesateach node in the system. The best fit estimate is the input into Step 3 to determine if there are any potential parameter errors in the system.

5.2.3 Step 3: Parameter Error Detection Algorithms and Equations

Parameter error identification is the process by which the measurement residuals from Step 2 are examined to determine if parameter errors exist [15]. Parameter errors are detected by identifying residuals with high sensitivity to a common device parameter. There are two approaches that are presented in this section.

5.2.3.1 Parameter Error Detection using the Sensitivity Matrix

The sensitivity of the measurement residuals to measurement errors is referred to as the Sensitivity Matrix (S) as given by (5.4) [9].

$$S = I - HG^{-1}H^{T}R^{-1} \tag{5.4}$$

From the sensitivity matrix, the covariance matrix is calculated as shown in (5.5).

$$\Omega = SR \tag{5.5}$$

Elements of covariance matrix indicate how strongly coupled measurements are. Additionally, the covariance matrix is used to normalize measurement residuals.

$$r_i^N = \frac{r_i}{\sqrt{\Omega_{ii}}} = \frac{z_i - h_i}{\sqrt{\Omega_{ii}}} \tag{5.6}$$

Normalized residuals can be used for the detection of bad measurements; if they are above the threshold of 3.0 the measurementis generally considered suspect. Additionally, normalized residuals can be used for the detection of bad parameters. If all of the normalized residuals of measurements sensitive to a particular parameter are high, an erroneous parameter value may be indicated. For example, if there are a number of high residuals in reactive power, but not real power, this could be an indication that the assumed value of capacitance for an underground cable is inaccurate. This concept will be examined more in Section 5.2.5.

5.2.3.2 Parameter Error Detection using Normalized Lagrangians

Normalized Lagrangians, λ, are an additional metric used to identify parameter error [16]. The SE problem is augmented in the classic Lagrangian fashion. The parameters in the system, p, are defined as $p = p_t + \varepsilon$, where p_t is the true network parameter and ε is the parameter error. The measurement vector z will then be expressed as $z = h(x, \varepsilon) + e$, where z is the measurement vector, h is the nonlinear function relating the measurement vector to the state vector and network parameters, x is the system state vector, and e is the vector of measurement errors. The parameter error vector is taken to be zero and can appear as an equality constraint on the state estimation problem.

As before, minimize the objective function $J(x)$:

$$J(x) = [z - h(x)]^{T}R^{-1}[z - h(x)] \tag{5.7}$$

but subject to the constraint:

$$\varepsilon = 0 \tag{5.8}$$

Forming the Lagrangian and applying first order optimality conditions leads to the classic SE equations as well as an additional set:

$$\frac{\partial L}{\partial \varepsilon} = H_{\varepsilon}^{T} R^{-1}(z - h) + \lambda = 0 \tag{5.9}$$

Where $H_{\varepsilon}^{T} = \frac{\partial h(x,\varepsilon)}{\partial \varepsilon}$ and λ is the Lagrange multiplier for the parameter error constraint. λ can be expressed as shown in 5.10.

$$\lambda = -\frac{\partial h(x,\varepsilon)}{\partial \varepsilon}^{T} R^{-1}(z - h) = -H_{\varepsilon}^{T} R^{-1}(z - h) = \psi(z - h) \tag{5.10}$$

A statistical test for detecting parameter errors based on λ can be developed. It is assumed that all Lagrange multipliers are distributed according to a normal distribution with zero mean and non-zero covariance. The covariance matrix can be derived following the relationship between the Lagrange multipliers and measurement residuals

$$\Lambda = cov(\lambda) = \psi \Omega \psi^{T} \tag{5.11}$$

Similarly to measurement residuals, the Lagrange multipliers can be normalized as

$$\lambda_i^N = \frac{\lambda_i}{\sqrt{\Lambda_{ii}}} \tag{5.12}$$

A typical threshold of 3.0 can be used to identify suspect parameter values.

5.2.3.3 Parameter Error Identification Summary

Whether using a sensitivity matrix or normalized Lagrangians, it is possible to identify suspect parameters from measured values. Both of these methods exist in the literature for balanced transmission systems, but have had limited use on distribution systems. This work has expanded the existing methods of parameter error to unbalanced distribution systems.

The output of this step is a list of device parameters that are identified as outside of the expected values indicated by the planning model. It is possible that multiple parameter errors will be identified, and it will need to be determined if all identified parameters can be estimated, given the limitations imposed by observability. Since AMI data is generally recorded on 5-minute or 15-minute intervals, there is sufficient time to track numerous parameters. While this can be used as an operational tool, the effects that are being examined happen over long time frames, so computational burdens should be low.

5.2.4 Step 4: Parameter Estimation and Tracking Algorithms and Equations

Once parameters have been identified as being outside of their expected values, the next step is to determine if the values are constant or time-varying. Parameters errors that are constant and parameter errors that are time-varying constitute two distinctly different scenarios. If a parameter

error is identified, and its value is constant, but outside of the expected value, it must be determined whether the source data is in error. For many utilities, the source data is the distribution planning models, which have many potential sources of error. These sources of errors can include, but are not limited to: errors from the import of the utility Graphical Information System (GIS), incorrect line lengths in the database, incorrect conductor types in the database, and incorrect cable types in the database. In any of these cases, a constant value parameter error can indicate an error in the source data. One option is to conduct an analysis to determine the best fit value of the parameter, and to use this as the new value in the source data. If this is done, it should be noted that this substitution has been made. If the value is time-varying, the time-varying characteristics must be compared to a model of expected behavior to see if the variation is within expected parameters, or an indication of a potential problem.

Presently two methods of tracking parameter errors are being examined. The first is a state augmentation based approach, and the second is an extension of the parameter error detection using the sensitivity matrix.

5.2.4.1 Parameter Tracking with Augmenting the State Vector

The suspected parameters are included in the state vector and both the states and parameters are simultaneously estimated. Several snapshots, or sets of measurements taken at the same time step, are aggregated and used for parameter estimation process. This is done in order to increase the local redundancy around suspect parameters and increase the accuracy of estimates of parameter values.

Except for some observability and numerical issues (e.g., risk of Jacobian singularity at flat start) this approach is an extension of the conventional SE model.

States are expressed as:

$$x = [\theta_2 ... \theta_n \quad V_1 ... V_n \quad p_{aram}]^T \tag{5.13}$$

$$x' = [\theta_2 ... \theta_n \quad V_1 ... V_n]^T$$

$p_{aram} = p_{aram,1} \cdots p_{aram,2}$ is the vector of estimated parameter values

$$h(x) = \left[P_i^p \quad Q_i^p \quad \cdots \quad V_i^p \cdots \right]^T \tag{5.14}$$

For a full three-phase model, a power injection measurement at bus i on phase p, P_i^p, involves a double sum, taken over all buses and all phases in similar terms to (5.3).

$$P_i^p = V_i^p \sum_{k=1}^{n} \sum_{q=1}^{3} V_k^q \left[G_{ik}^{pq} \cos\theta_{ik}^{pq} + B_{ik}^{pq} \sin\theta_{ik}^{pq} \right] \tag{5.15}$$

The corresponding measurement Jacobian is given by:

$$H(x) = \frac{\partial h(x)}{\partial x} \tag{5.16}$$

The Jacobian has two components, as shown in Eq.(5.17): one is the derivative of *h* with respect to states (5. 18), the other one is the derivative of *h* with respect to parameters (5.19).

$$H(x) = \begin{bmatrix} H(x') & H(p_{aram}) \end{bmatrix} \tag{5.17}$$

$$H(x') = \begin{bmatrix} \frac{\partial h_1}{\partial \theta_{2a}} & \frac{\partial h_1}{\partial \theta_{2b}} & \frac{\partial h_1}{\partial \theta_{2a}} & \cdots & \frac{\partial h_1}{\partial \theta_{na}} & \frac{\partial h_1}{\partial \theta_{nb}} & \frac{\partial h_1}{\partial \theta_{nc}} & \frac{\partial h_1}{\partial V_{1a}} & \frac{\partial h_1}{\partial V_{1b}} & \frac{\partial h_1}{\partial \theta_{1c}} & \cdots & \frac{\partial h_1}{\partial V_{na}} & \frac{\partial h_1}{\partial V_{nb}} & \frac{\partial h_1}{\partial V_{nc}} \\ \frac{\partial h_2}{\partial \theta_{2a}} & & & & & & & & & & & & & \vdots \\ \vdots & & & & & & & & & & & & & \\ \frac{\partial h_m}{\partial \theta_{2a}} & \cdots & & & & & & & & & & & \cdots & \frac{\partial h_m}{\partial V_{nc}} \end{bmatrix} \tag{5.18}$$

$$H(p_{aram}) = \begin{bmatrix} \frac{\partial h}{\partial p_{aram,1}} \cdots \frac{\partial h}{\partial p_{aram,n}} \end{bmatrix} = \begin{bmatrix} \begin{bmatrix} \frac{\partial h_1}{\partial p_{aram,1}} \\ \frac{\partial h_2}{\partial p_{aram,1}} \\ \vdots \\ \frac{\partial h_3}{p_{aram,1}} \end{bmatrix} \cdots \begin{bmatrix} \frac{\partial h_1}{\partial p_{aram,1}} \\ \frac{\partial h_2}{\partial p_{aram,1}} \\ \vdots \\ \frac{\partial h_3}{p_{aram,1}} \end{bmatrix} \end{bmatrix} \tag{5.19}$$

In practice, in order to perform state estimation more frequently and perform the parameter estimation less frequently, in other words, to estimate states with relatively constant parameters, we deploy a stacking method.

Multiple previous state estimation results are stacked into a large matrix to estimate a set of parameters. The size of the Jacobian, state, and measurement matrices are expanded. Eq. (5. 17) is expanded as follows:

$$H_{stack}(x_{stack}) = \begin{bmatrix} H_1(x'_{1SE}) & & H_{p1}(p_{aram}) \\ & \cdots & \vdots \\ & H_w(x'_{wSE}) & H_{pw}(p_{aram}) \end{bmatrix} \tag{5.20}$$

where *w* is the number of state estimations and also the width of a moving window.

The moving time step is the time interval between two snapshots. At the completion of the stacked state estimation there will be *w* sets of voltage state estimates and a set of single

parameter estimates. Thus, the parameter estimate is the best fit for all time points stacked as an input for the estimator.

5.2.4.2 Parameter Tracking based on Residual Sensitivity Analysis

An alternate method of estimating parameter errors can be performed separately from State Estimation in an external loop. After a SE is performed, the vector of measurement residuals, r, sensitivity matrix, S, and Jacobian with respect to parameters, $\frac{\partial h(x,p)}{\partial p}$, can be computed. The parameter error can be computed from these quantities in the following fashion.

The sensitivity matrix, *S*, calculated in Eq. 5.4, also gives the relationship between residuals and measurement errors, $r = Se$. A linear relationship can be found between measurement residuals and parameter error:

$$r_s = \left(S_{ss}\frac{\partial h_s}{\partial p}\right)\varepsilon + \overline{r_s} \tag{5.21}$$

where $S_{ss}$is the submatrix of *S* corresponding to *s* involved measurements and $\overline{r_s}$ is the residual that would have been found if the parameter were correct. The relationship given in Eq. 5.21 can be interpreted as a local estimation problem and the optimal value of ε in the least squares sense can be computed:

$$\varepsilon = \left[\left(\frac{\partial h_s}{\partial p}\right)^T R_s^{-1} S_{ss}\left(\frac{\partial h_s}{\partial p}\right)\right]^{-1}\left(\frac{\partial h_s}{\partial p}\right)^T R_s^{-1} r_s \tag{5.22}$$

The estimated error can then be used to update the parameter value in the system model [9].

If multiple sets of measurements are available, as they would be in the case of AMI data, the parameter can be estimated more robustly by considering many measurement sets together. The measurement residual vectors can be concatenated, as can the *S*, *R*, and $\frac{\partial h}{\partial p}$ computed at each solution of the SE process. The parameter error can be computed from these augmented inputs, either at each timestep, using data from a moving window, or once per some multiple of measurement timesteps.

5.2.4.3 Parameter Tracking Summary

Regardless of which of the two methods is used, the output from Step 4 is a plot showing the variation of a parameter(s) of interest over time. These time-varying values are the output of Step 4 and are the input data for Step 5.

5.2.5 Step 5: Cable/Transformer Diagnostic Algorithms and Equations

As discussed in section 5.2.3.1, it is possible to use groups of high-valued normalized residuals to identify what specific equipment parameter is in error. For example, if multiple real power injections are identified as parameter errors, but not reactive power injections or voltage

magnitudes, the self-impedance of an overhead line, $\hat{Z}_{ii}$, may be the cause. The self-impedance of an overhead line is given by 5.23 [17].

$$\hat{Z}_{ii} = r_i + 0.9530 + j0.12134\left(ln\left(\frac{1}{GMR_i} + 7.79402\right)\right) ohm/mile \quad (5.23)$$

where:

r_i : Resistance of the phase conductor
GMR : Geometric Mean Radius

If the self-impedance of a line, $\hat{Z}_{ii}$, is identified as a time-varying parameter error, equation 5.23 shows that the source of the variation must track to the resistance, r_i, since r_i is the only value that is not a fixed geometric constant. Assuming fixed geometric values for an underground cable is reasonable since the only way for them to change would result in mechanical damage to the cable that would result in catastrophic damage.

Similar to the overhead line, if the capacitance of an underground cable is identified through parameter errors this can be correlated to a physical characteristic of the cable; specifically the insulation jacket. Equation (5.24) shows the correlation between the capacitance of a concentric neutral cable and the insulating jacket [17].

$$C_{pg} = \frac{2\pi\varepsilon_0\varepsilon_r}{ln(R_b/RD_c) - (1/k)ln(kRD_s/R_b)}\mu S/mile \quad (5.24)$$

where:

ε_0 : Permittivity of free space
ε_r : Permittivity of material (insulating jacket)

Once again, similar to the overhead line, variations in the capacitance of the capable can be tracked directly to the permittivity of the insulating material, ε_r. In both cases, the variation of overhead line resistance and the dielectric properties of cable insulating jackets over time are well understood. Comparing the values as tracked over time to what is expected based on known models will form the basis for determining if the distribution system elements need to be replaced.

5.3 Simple Example Case

The process described above has been applied to a modified IEEE Test System; the 13 Node Test Feeder. This section contains results of algorithms described in Section 5.2 carried out on that model system.

5.3.1 Model System

The model system was a modified version of the IEEE 13 Node Test Feeder [18]. Simplifications were made to the original IEEE test feeder to focus the simulations on the core interest of state and parameter estimation. A switch, the regulator, and transformer were not modeled. And, a delta load was transformed into a Y load. The schematic of the feeder used in the simulations described in this section can be seen in Figure 5.2 below. Note, node numbers and phases are labeled in the figure.

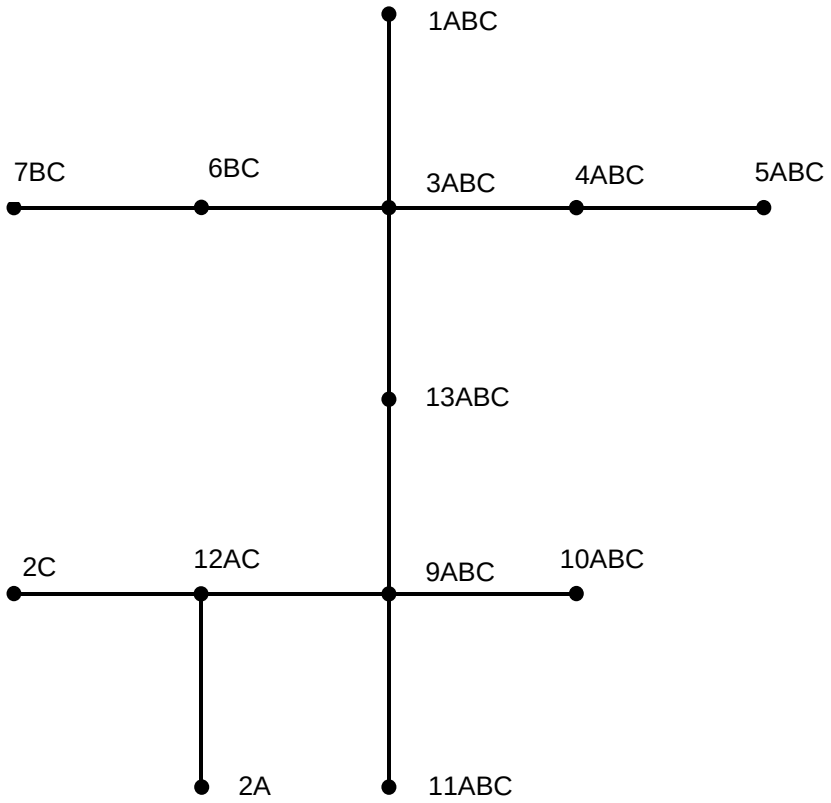

Figure 5.2: Schematic of distribution feeder used in test cases

In order to streamline the process of preparing input data for the state estimation and parameter estimation procedures, as well as to facilitate the generation of multiple measurements/timesteps, the test network was constructed in an input format for GridLAB-D. Whether for a single time step or a one-year set of data, GridLAB-D was used to create perfect (no noise) measurement sets with real power injection, reactive power injection, and voltage magnitude for every bus at every time step. GridLAB-D was also configured to output a data structure containing the network impedance data in a form acceptable for the state and parameter estimation procedures. This data structure included primitive three-phase impedance matrices for each link in the system. Supplementary scripts were written to parse the measurement data and add noise/error where appropriate, as well as to construct a formal three-phase admittance matrix from the primitive impedance data. This process is outlined below in Figure 5.3.

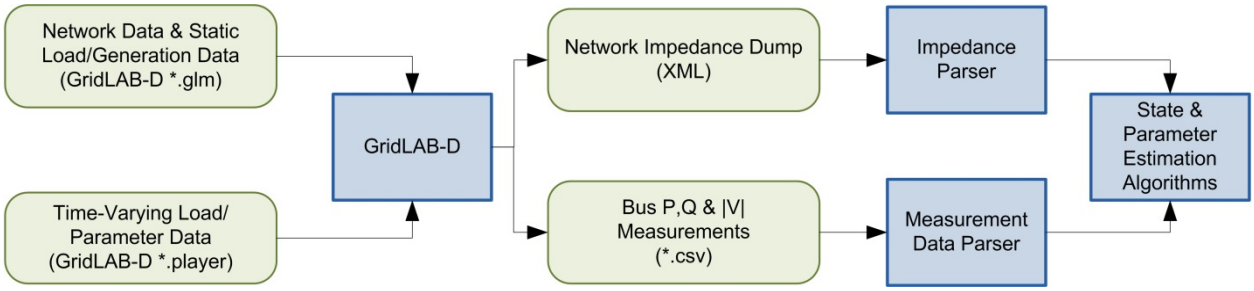

Figure 5.3: GridLAB-D Data Collection and Processing Flow

5.3.2 State Estimation

Using the algorithm described in Section 5.2.2, a state estimation was performed using simulated measurements generated by GridLAB-D. There are a wide variety of ways to evaluate the performance of a state estimator. One common way is to compare the estimated values of the state vector to the true values, which can be computed when there is perfect knowledge of the system, as in a simulation experiment. For a system with N voltage magnitude elements in the state vector, define the average absolute value in the estimation to be

$$S_{|V|} = \frac{1}{N}\sum_{i=1}^{N} |V_t - V_{est}| \tag{5.25}$$

where V_t is the true value of the voltage magnitude as solved by power flow, and V_{est} is the voltage magnitude estimated by the state estimator. Similarly, for voltage angle,

$$S_\theta = \frac{1}{N}\sum_{i=1}^{N} |\theta_t - \theta_{est}| \tag{5.26}$$

If no simulated measurement error is induced, the per-unit $S_{|V|}$ is less than $5\text{x}10^{6}$ and the value of S_θ is less than $2\text{x}10^{6}$. These values are at the limit of accuracy given the precision of the simulated measurements, proving the successful operation of the three phase state estimator.

5.3.3 Parameter Error Detection

The parameter error detection methods were tested by taking the system data generated by GridLAB-D and introducing an erroneous value. The parameter ‘R1-3aa’ refers to the real part of the direct *a*-phase element of the 3x3 impedance matrix that describes the characteristics of the line linking node 1 and node 3. That parameter was set to several erroneous values, and the methods described in Section 5.2.3 were applied to detect the error. Below the normalized measurement residuals and normalized Lagrangian are plotted as a function of fractional parameter error. In this case, R1-3aa was set to a variety of erroneous values and then the parameter error detection algorithms were carried out after the SE had completed.

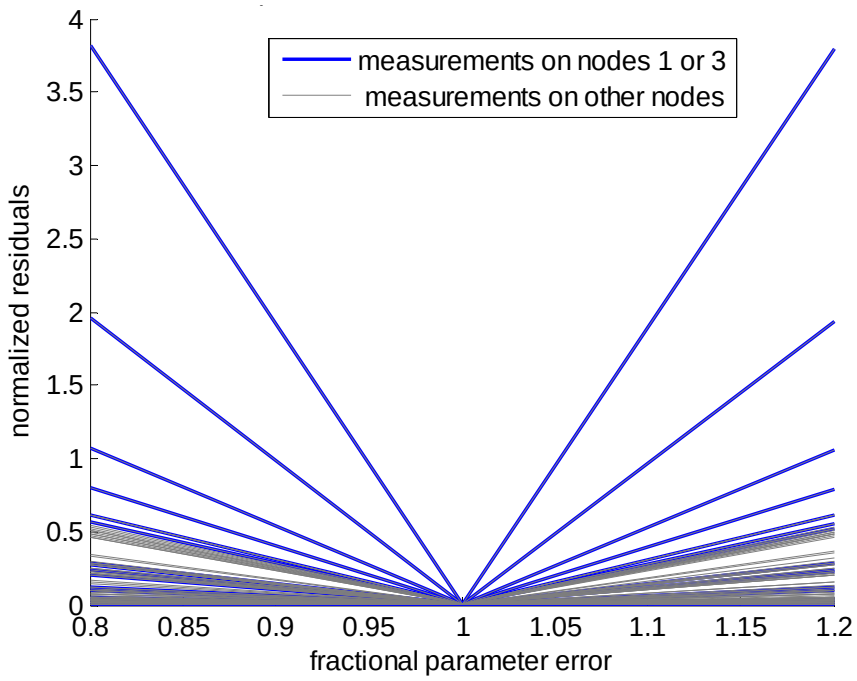

Figure 5.4: Effect of error induced on parameter R1-3aa on normalized measurement residuals

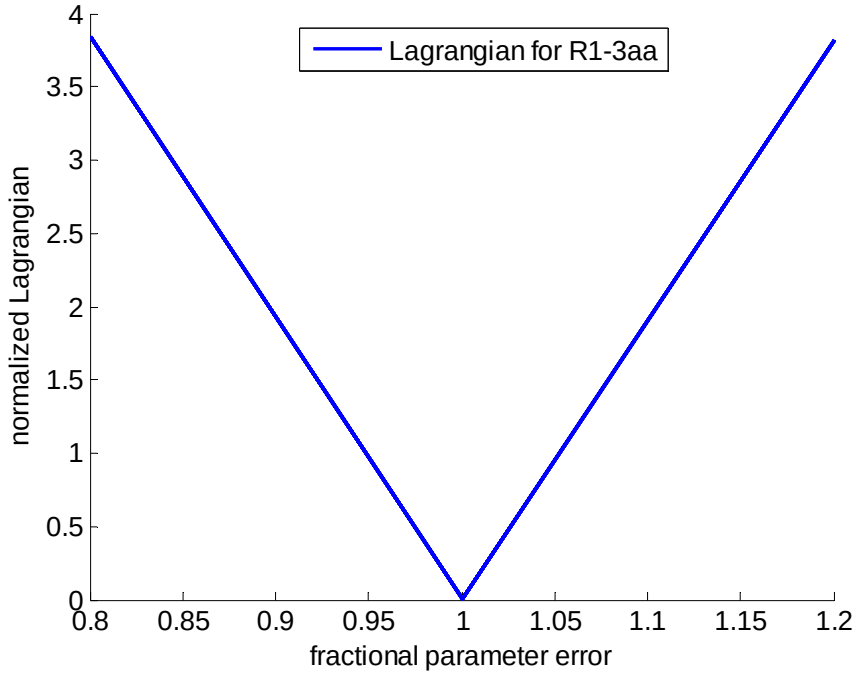

Figure 5.5: Effect of error induced on parameter R1-3aa on normalized Lagrangian

As can be seen in the figures above, an induced parameter error of 15% is sufficient to raise either the measurement residuals or the normalized Lagrangian above the detection threshold of 3.0. The normalized Lagrangians are made up of linear combinations of measurement residuals, scaled by the strength of influence that a given parameter has on a measurement. In this particular case, the normalized Lagrangian displays a similar degree of sensitivity to parameter error as the most sensitive normalized measurement residual, but that is not true in all cases.

The normalized Lagrangian method has the additional advantage that multiple state estimations can be performed at successive points in time, and then the outputs of each can be concatenated to calculate a single normalized Lagrangian, increasing the sensitivity.

5.3.4 Parameter Estimation

The value of an unknown or erroneous parameter was estimated for multiple test cases using both of the techniques described in Section 5.2.4. The cases are of both static and time-varying. The static cases are used to exemplify some of the details that are not visible when multiple time points are plotted. The analysis of results from time-varying cases is focused on the ability to track parameter changes through time.

To examine ability to detect changes in parameter of line charging, an exponentially growing shunt capacitance was added to the model at node 13. The expectation is that this parameter will change as an underground cable reaches end of life. The system data that was used for state estimation contained a small and constant shunt capacitance, and the exponentially growing shunt capacitance could be detected and estimated by both methods shown below.

5.3.4.1 Parameter Estimation with Augmenting the State Vector

The parameter error estimation technique described in Section 5.2.4.1 is deployed and implemented. Case studies are carried out to test the methodology of parameter estimation, which are:

- Single parameter and single snapshot
- Multiple parameters and two snapshots
- Single parameter and time series snapshots with no growth of shunt capacitance
- Time series snapshots with exponential growth of shunt capacitance

The case study results are presented and discussed in this section.

5.3.4.1.1 Single Parameter and Single Snapshot

In this case, R1-3aa, a critical resistance on an upstream line, is estimated individually and the estimated parameter values change with iterations, as presented in Figure 5.6. The initial value was set to double the true value of R1-3aa (i.e. the initial value is 0.1518 p.u.). The true value is 0.0759 p.u., so the error was 0.0759 initially. After 4 iterations, the estimated error, the difference between the estimated value and the true value, merged to zero.

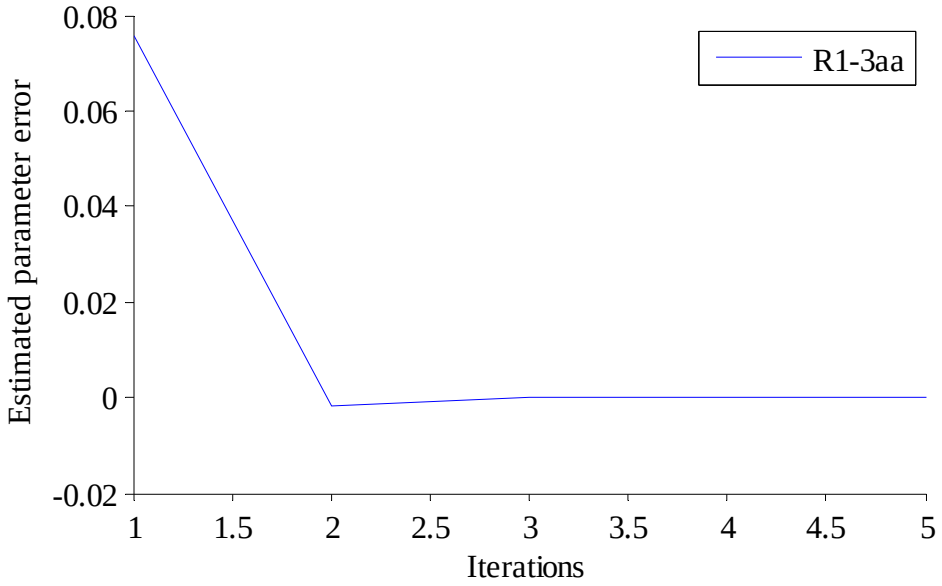

Figure 5.6: Estimated error on parameter R1-3aa at one snapshot

5.3.4.1.2 Multiple Parameters and Two Snapshots

It requires 8 iterations to converge for estimating 6 parameters simultaneously. Afterwards, it read the second snapshot as a new measurement data set with a step change in the R1-3aa. The estimated value of R1-3aa converged to a new value (which is the new true value). In Figure 5.7, there is a step change in the estimate error, which is a differential from the original true value. The difference can be observed after the 9th iteration. This method can estimate step changes on R1-3aa.

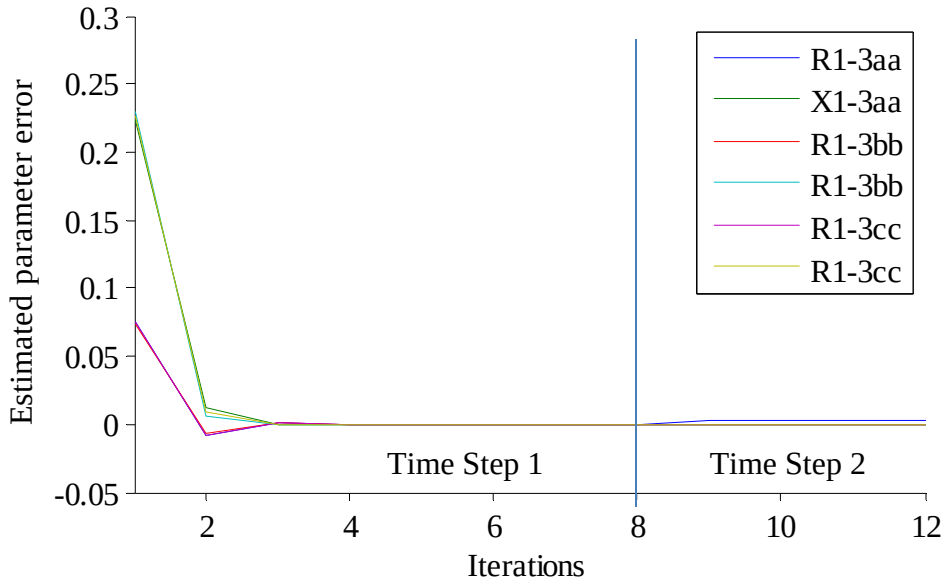

Figure 5.7: Estimated error on multi-parameters at two snapshots

5.3.4.1.3 Single Parameter and Time Series Snapshots with No Change in Shunt Capacitance

In this case, there is no change in shunt capacitance at node 13. B139aa is estimated based on hourly time series measurement data set. All system parameters remain constant while the measurement data changes with time increasing. Figure 5.8 indicated there are many noises in the estimated values. A linear fit which gets rid of the oscillations of the estimated values is also shown in Figure 5.8.

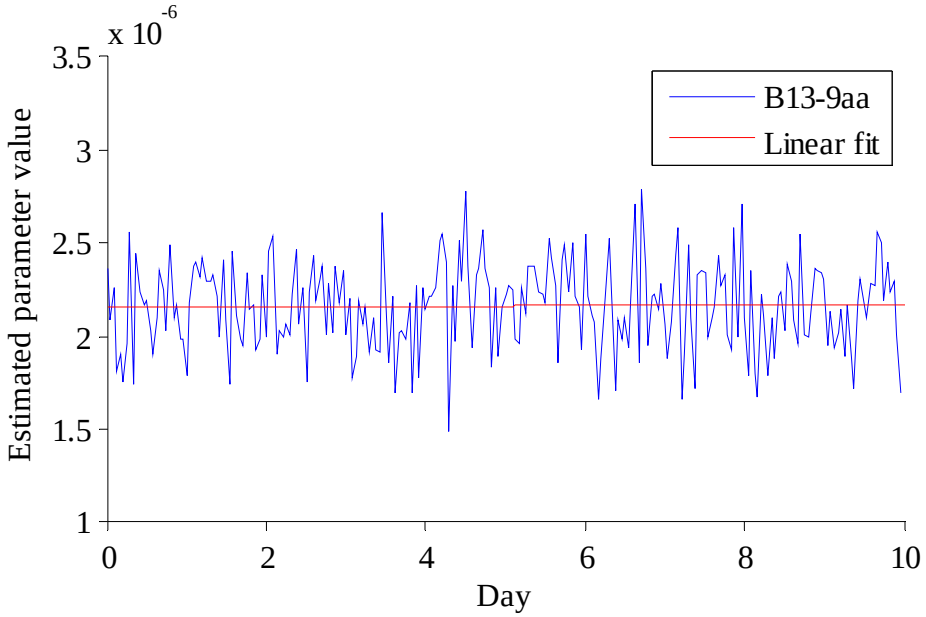

Figure 5.8: Estimated error on parameter B13-9aa at one snapshot

5.3.4.1.4 Time Series Snapshots with Exponential Growth of Shunt Capacitance

Based on the time series snapshots with exponential growth of shunt capacitance at node 13, parameter B13-9aa, B13-9bb, and B13-9cc are estimated simultaneously, as shown in Figure 5.9. It can be observed that the estimated parameter values increased significantly within the 54 days.

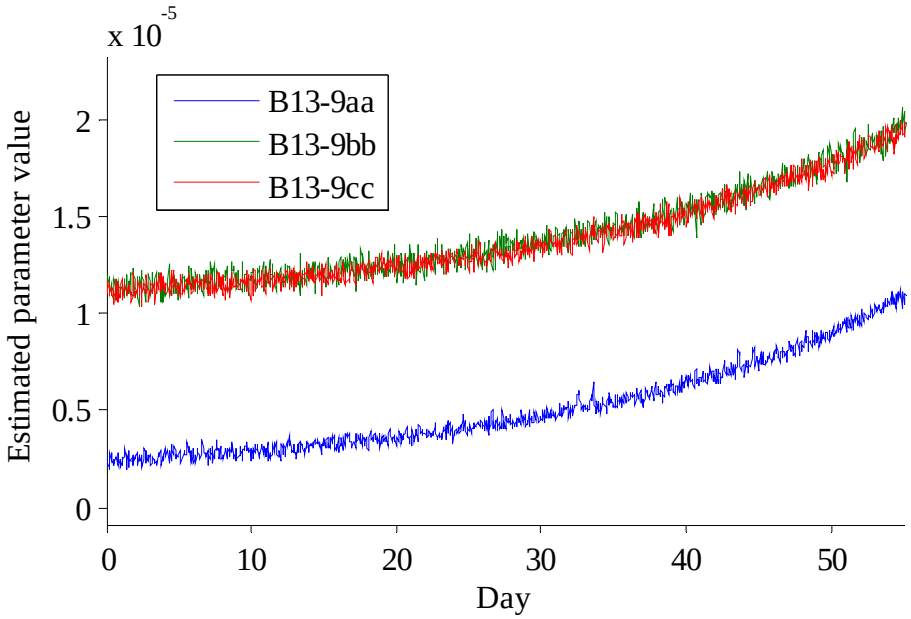

Figure 5.9: Estimated values of parameter B13-9aa, B13-9bb, and B13-9cc

Next, we use a stacking method as described in Section 5.2.4.1. The solutions of the 24 (i.e., 1 day of hourly snapshots) previous state estimations are stacked into a large matrix to estimate a set of parameters. The size of Jacobian, state, and measurement matrices are expanded. With the previous 24 hours state estimations input, the parameters are estimated at each snapshot. In another word, 24 hours is the width of a moving window and the moving time step is one hour. States are estimated hourly for 24 hours and parameters are estimated at the end of these 24 hours. Each parameter estimation process requires 24 previous state estimation snapshots.

The true values of R1-3aa, R1-3bb, and R1-3cc are 0.07585, 0.07386, and 0.074720. Using the state augmenting and the stacking method, R1-3aa, R1-3bb, and R1-3cc are correctly estimated simultaneously and remain constant for 30 days, as shown in Figure 5.10.

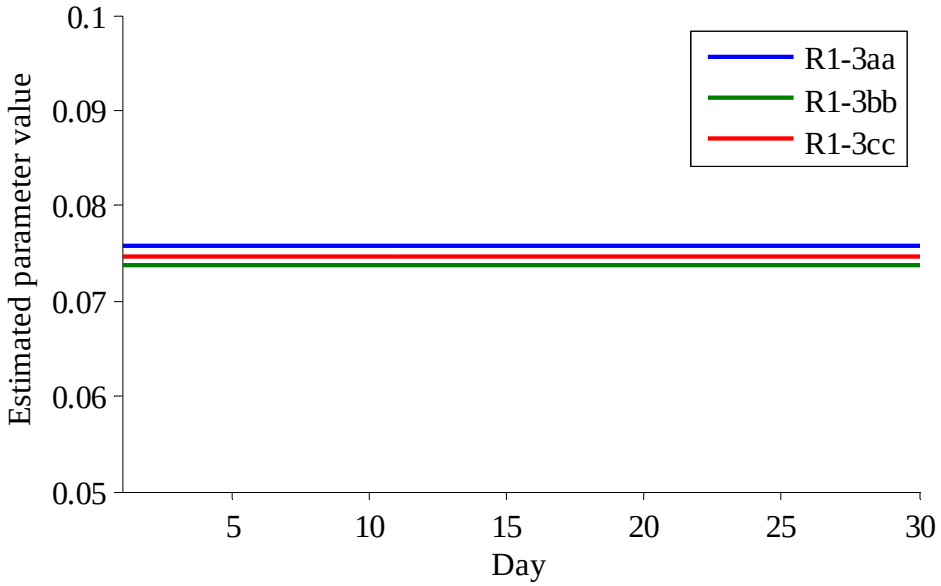

Figure 5.10: Estimated error on parameter R1-3aa, R1-3bb, and R1-3cc for 30 days

A comparison of two results of B13-9aa parameter estimation with and without a stacking window is shown in Figure 5.11. Obviously, the stacking method reduces the noise associated with estimated values of B13-9aa and both of them present the exponential growth as time increases.

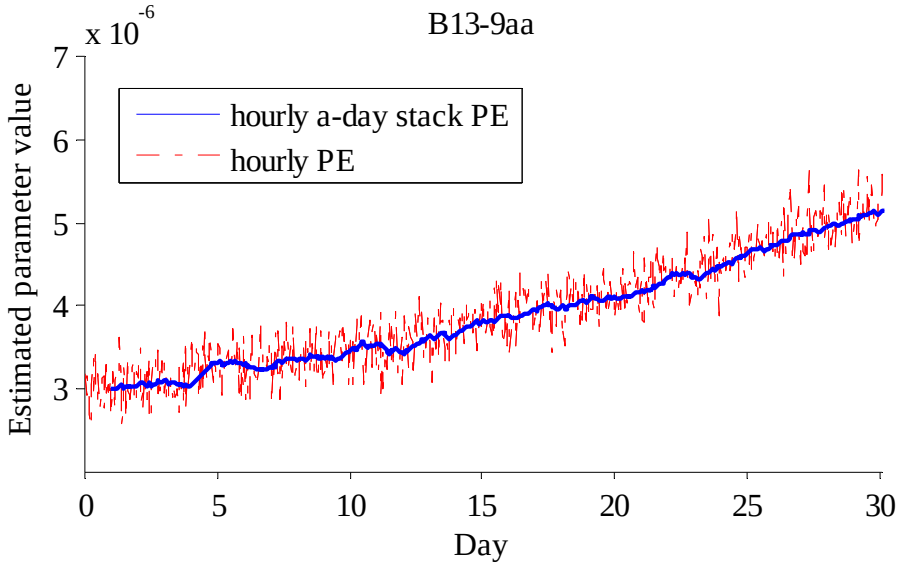

Figure 5.11: Comparison of estimated values of parameter B13-9aa

Figure 5.10 and Figure 5.11 show that this parameter estimation method can detect increase in shunt capacitance B13-9aa without taking R1-3aa, R1-3bb and R1-3cc as suspects. They indicate that parameter estimation can provide early warnings to system operators before they observe abnormal values from the measurements.

5.3.4.2 Parameter Estimation Based on Residual Sensitivity Analysis

The parameter error estimation technique described in Section 5.2.4.2 was applied to several test cases. The cases included linear changes in series resistivity and exponential growth in shunt capacitance. The exponential shunt model case is the data set as used in 5.3.4.1.4.

5.3.4.2.1 Error Induced to Line Resistivity

In this case, error is induced in the parameter R1-3aa, as discussed in the Section 5.2.3, and the parameter error is then estimated using residual sensitivity analysis. The estimated parameter value is plotted on top of the induced parameter error in Figure 5.12 showing excellent agreement. In general, in this test system, the estimation for line resistance and reactance parameters is quite good.

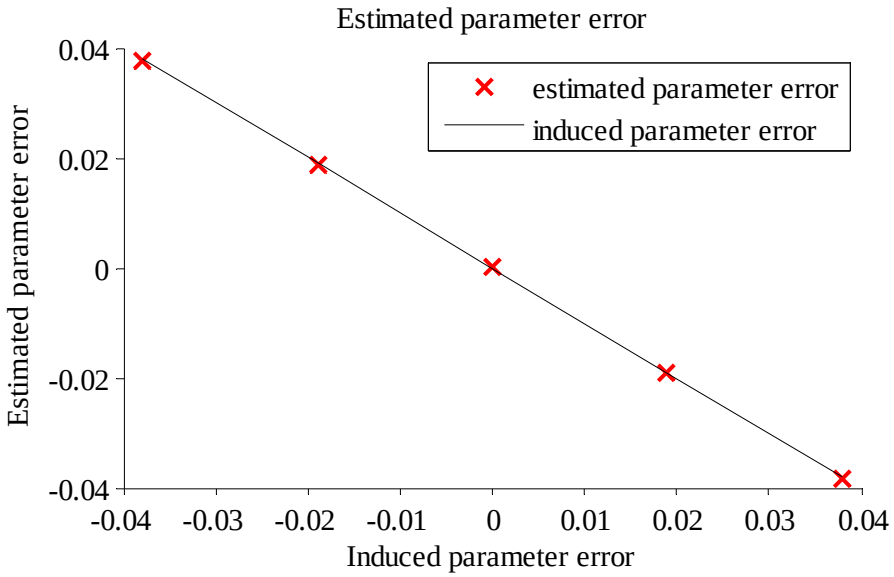

Figure 5.12: Estimated error on parameter R1-3aa

Because the residual sensitivity analysis method of estimating parameter errors is based on a linear approximation, the method works better for small errors, and begins to break down when parameter errors are large enough to cause serious error in the SE process. Additionally, since parameter errors are estimated one at a time, based on SE results, in a non-iterative fashion, an error in one parameter can sometimes affect the estimated of error in a very closely related parameter.

5.3.4.2.2 Exponential growth of shunt capacitance

The shunt capacitance in a typical system will be small on the scale of other parameters in the system. In the per-unit system used in these calculations, the shunt capacitance values are on the

order 10^{-6}, whereas line resistance and reactance are on the order 10^{-1}. This extremely small value makes accurate estimation difficult, and it can be seen that at the very beginning of the simulation, there is not good agreement because the actual and estimated value. In the case shown below, the value of the shunt capacitance was $1x10^{-6}$ at day 0 and $1x10^{-5}$ at day 53. In spite of the inaccuracy of the estimated value, the exponential growth trend is still clearly evident. The plotted parameter estimate was computed by taking a day of simulated AMI measurements, or 48 snapshots in time, and combining the results of each snapshot's state estimation for a single parameter estimation. The same method applied to closely related parameters, the line resistivity on a link connecting to node 13, shows the expected null result. When the shunt capacitance was increased, the estimate of error on line resistivity remains near zero.

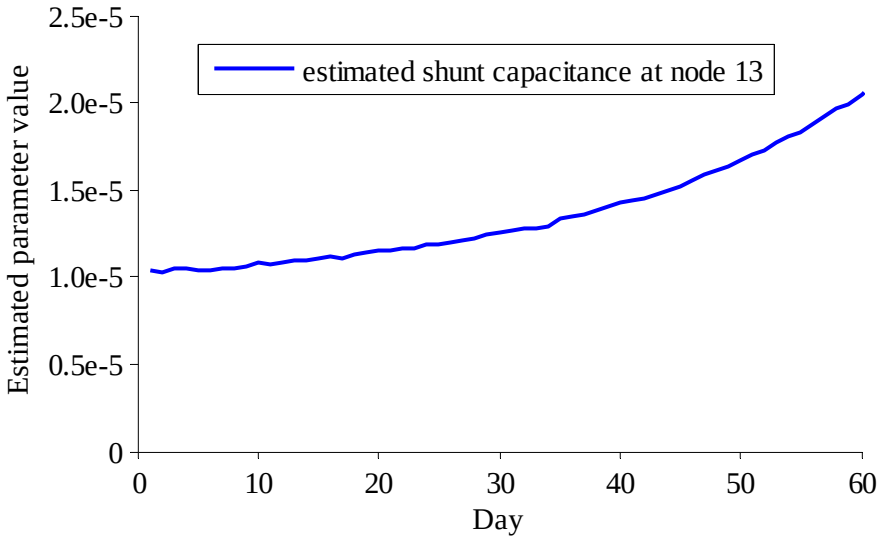

Figure 5.13: Estimated shunt capacitance as a function of day.

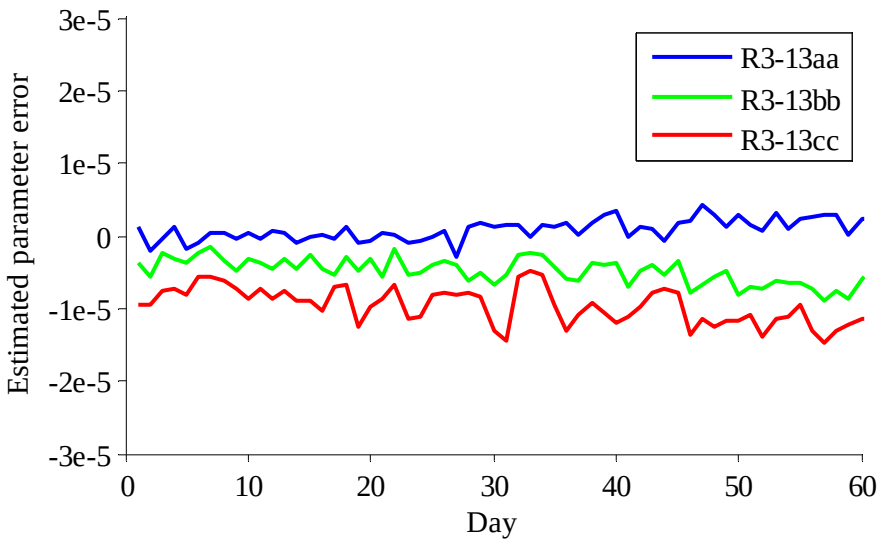

Figure 5.14: Estimated error of nearby line resistivity parameters.

5.4 AMI State Estimation and Parameter Estimation Conclusion

Section 5 has detailed the developed of an AMI based diagnostics system for transformers and underground cables. In the process traditional state and parameter estimation techniques have been expanded to function on unbalanced 3-phase distribution systems. The developed AMI system allows a utility to identify transformers and underground cables that are deteriorating at faster than expected rates, and to take action. This capability will reduce unplanned outages to end-use customers and provide for a more informed asset management system. This diagnostic system works with a utilities existing AMI and communications infrastructure; this minimizes cost of implementation.

We expect as more smart devices (i.e., switches, shunts, and regulators) are installed, there will be increased telemetry on the branch power flows of the feeders. This will only improve the state estimation and parameter estimation performed, and therefore the identification of degrading transformers and underground cables.

We know that in future work using “real world” data, other states will need to be added, including such things as taps on voltage regulators and capacitor statuses. Next year we will continue to investigate how parameters of equipment change as end of life nears. We are presently working with utilities to obtain AMI data and feeder models to verify the results using a real system.

6 Concluding Comments

This document has detailed the four analysis capabilities that PNNL has developed in FY13. Each of the analysis capabilities supports the DOE/OE smart grid and microgrid program goals, shown earlier in the document. By 2020, DOE/OE expects smart grid research to allow a 20% reduction in SAIDI, 20% reduction in load factor, and a 98% or greater reduction in outages. For microgrids specifically, the 2020 goals include obtaining cost parity with diesel generators and UPS system, a 20% improvement in efficiency, 98% or greater reduction in outages, and 20% or greater reduction in emissions. The FY13 GridLAB-D analysis tasks provide underlying tools and initial capabilities to help meet these goals.

The FY13 recovery and restoration task with WSU produced a model and initial implementation of a reconfiguration algorithm. These provide a basis for analyzing the benefits of the reconfiguration approaches, as well as help evaluate any concerns operating the Pullman system as a microgrid. These benefits and concerns are a first step in evaluating if operating the Pullman system as a microgrid will reduce outage lengths (for longer outages) and operate the system more efficiently and with lower emissions. The FY14 work will refine the reconfiguration approaches to help maximize these DOE/OE goals.

The modeling framework produced a process for taking hardware devices and modeling them within a software environment. This allows for evaluation and refinement of proposed microgrids equipment and infrastructure before deployment, to help insure they are meeting the 2020 goals. While the direct development of this framework effectively concludes in FY13, further refinements will be made through its continued use. Seattle University will deploy the framework in their senior-level capstone engineering course and provide relevant feedback. The continued WSU work will utilize the framework as a means for improving the models of the WSU generation resources.

The GridLAB-D and TMO integration further enhanced the optimization that the TMO software provides by including electrical feasibility constraints. The TMO software is expected to be utilized heavily for evaluating and designing microgrid systems, including how each microgrid meets the DOE/OE microgrid goals. While the PNNL involvement in the task is effectively ending with FY13, SNL plans to demonstrate the TMO software during a November meeting, which may require some further development and refinement.

The AMI diagnostics project showed initial viability for utilizing existing measurement devices to help track system states and parameter changes in the equipment. Detecting parameter changes associated with pending equipment failures or system operational changes can be useful for both smart grid and microgrid aspects of operation. Knowing where a cable is getting ready to fail can prompt repairs before a costly outage, as well as pointing out potential weak-points in a reconfiguration into a microgrid. In either situation, the outages can be avoided or have a reduced impact. Work will continue into FY14 to evaluate field AMI data, as well as refine the algorithm for detection of other power system characteristics.

References

[1] United States Department of Energy, Office of Electricity Delivery and Energy Reliability, "2012 DOE Microgrid Workshop Summary Report". [Online]. Available: http://www.energy.gov/sites/prod/files/2012_Microgrid_Workshop_Report_09102012.pdf. Accessed September 25, 2013.

[2] Stanovic, A., S.R. Sander, and T. Aydin, "Dynamic Phasors in Modeling and Analysis of Unbalanced Polyphase AC Machines," *IEEE Transactions on Energy Conversion*, vol. 17, no. 1, pp. 107-113, 2002.

[3] GridLAB-D contributors, "Dynamic Phasor Implementation". [Online]. Available: http://sourceforge.net/apps/mediawiki/gridlab-d/index.php?title=DynamicPhasor, accessed September 24, 2013.

[4] GridLAB-D contributors, "Modeling Framework". [Online]. Available: http://www.gridlabd.org/flowchart.stm, Accessed September 24, 2013.

[5] GridLAB-D contributors, "Subsecond Inverter Specifications". [Online]. Available: http://sourceforge.net/apps/mediawiki/gridlab-d/index.php?title=Spec:SubsecondInverter, Accessed September 24, 2013.

[6] R. Hartlein and N. Hampton, "Diagnostic Testing of Underground Cable Systems," 2010.

[7] W. Thue, Ed., *Electric Power Cable Engineering*, Third. CRC Press, 2012.

[8] M. Baran, J. Jung, and T. McDermott, "Including voltage measurements in branch current state estimation for distribution systems," Power and Energy Society General Meeting, no. 1, pp. 1–5, 2009.

[9] A. Abur and A. Exposito, *Power system state estimation: theory and implementation*. 2004.

[10] M. Mashikian, "Preventive diagnostic testing of underground cables," … Conference and Exposition, 2001 IEEE/PES, 2001.

[11] F. C. Schweppe, "Power System Static-State Estimation, Part I: Exact Model," *IEEE Transactions on Power Apparatus and Systems*, no. 1, pp. 120–125, 1970.

[12] F. Schweppe and D. Rom, "Power System Static-State Estimation, Part II: Approximate Model," *IEEE Transactions on Power Apparatus and Systems*, vol. PAS-89, no. 1, pp. 125–130, Jan. 1970.

[13] F. Schweppe, "Power system static-state estimation, Part III: Implementation," *IEEE Transactions on Power Apparatus and Systems*, no. 1, pp. 130–135, 1970.

[14] C. W. Hansen and A. S. Debs, "Power System State Estimation Using Three-Phase Models," *IEEE Transactions on Power Systems*, vol. 10, no. 2, pp. 818–824, 1995.

[15] A. Abur and J. Zhu, "Identification of parameter errors," Power and Energy Society General Meeting, 2010 IEEE. pp. 1–4, 2010.

[16] J. Zhu and A. Abur, "Identification of network parameter errors," *Power Systems, IEEE Transactions on*, vol. 21, no. 2. pp. 586–592, 2006.

[17] W. Kersting, *Distribution system modeling and analysis*. 2012.

[18] W. Kersting, "Radial distribution test feeders," Engineering Society Winter Meeting, 2001. IEEE, 2001.

PNNL-22813

Pacific Northwest
NATIONAL LABORATORY

Proudly Operated by Battelle *Since 1965*

U.S. DEPARTMENT OF
ENERGY

902 Battelle Boulevard
P.O. Box 999
Richland, WA 99352
1-888-375-PNNL (7665)
www.pnnl.gov